Part IV:

Space Radiation

Chapter 17

Ionizing Radiation

Donald E. Robbins, Vladislav M. Petrov, Walter Schimmerling, and Igor B. Ushakov

Exposure to ionizing space radiation is one of many hazards associated with human exploration of space. Although other risks exist, efforts to limit exposures of spacecraft occupants clearly affect mission planning, and could well be the limiting factor in future extended orbital and exploration missions. Space radiation and its associated risks have been recognized by both the U.S. and Russian space programs,[1-6] and radiation standards and risk assessments for complex extended missions have evolved over the last three decades.[6-10] Because space ionizing radiation presents a unique risk, space travelers have been monitored carefully, from both experimental and operational perspectives, since the earliest orbital space missions.[11-13]

I. Sources of Radiation in Space

Primary sources of ionizing space radiation include the trapped-radiation belts, galactic cosmic rays (GCR), and solar particle events (SPE). Secondary radiation, which includes neutrons, also is produced when primary radiation interacts with the material media of the spacecraft, its human occupants, or constituents of the upper atmosphere. These sources are described below.

A. Trapped Belt Radiation

The trapped-radiation belts were discovered in 1958 by large Geiger counters that were part of a cosmic ray experiment on the first U.S. satellite, Explorer I. Their existence was confirmed by later measurements on Explorer III and first reported by Van Allen[14] in 1960.

Charged particles in these belts are constrained to move along magnetic field lines by the Lorentz force, F

$$F = (dp/dt) = qv \times B$$

where q, v, and p are the charge, vector velocity, and vector momentum of the particle; B is the vector magnetic-flux density; and the differentiation is with respect to time t. Trapped-particle motion can be understood as a superposition of three fundamental components: a gyration around the field line, a bounce from one polar region to the other, and a longitudinal drift around the Earth (Fig. 1).

Since the energy of a charged particle is not affected by a static magnetic field, its magnetic moment μ is an adiabatic invariant

$$\mu = mv \sin(\alpha/2B)$$

where α is the particle's pitch angle (the angle between its velocity vector v and the magnetic field vector B). The mirror point B_m of the particle (where it reverses direction of motion) can be obtained from

$$B_m = (B/\sin^2\alpha) = \text{constant}$$

where α is p/2.

A particle traces a magnetic shell of motion as it moves about the Earth. The shell is defined by an integral adiabatic invariant, I

$$I = \dot{U}\, dl \sqrt{1 - (B/B_m)}$$

where B is the flux density along the line of force and the integral is taken along a line of force.

Early attempts to fit measurements of trapped-radiation intensities by using a simple dipole representation of the Earth's magnetic field were unsuccessful. As a consequence, McIlwain[15] developed a two-dimensional coordinate system based on magnetic-field strength B and a parameter L related to the radial position of a particle. The B and L coordinates can be derived from conditions of the static magnetic field in the absence of an electric field. The magnetic field can be described in terms of a scalar potential ψ

$$B = -\Delta\psi$$

where

$$y = -(M \times r / r^3)$$

M, the vector magnetic moment of the dipole, is oriented in the negative z direction, and r is the position vector from the center of the Earth. (The magnitude of the Earth's magnetic moment is 8.1×10^{25} gauss cm^3.) In spherical polar coordinates, the magnetic field strength is

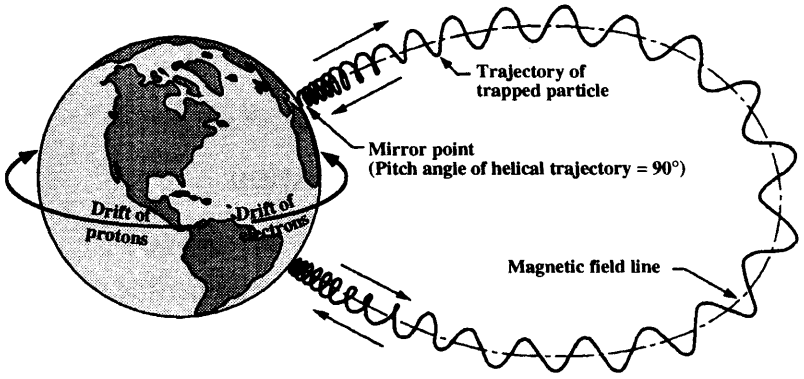

Fig. 1 Artist's conception of the motion of a trapped charged particle along Earth's magnetic field line.

$$B = B_o(R_o / r)^3\sqrt{4-(3r/L)}$$

where B_o is the magnetic flux density at the equatorial surface of the Earth (0.32 gauss), R_o is the radius of the Earth (6371.2 km), and L is given by

$$L = (r/\sin^2\theta)$$

where θ is the angle between the z axis and the position vector r.

Figure 2 shows the regions of the Earth's magnetosphere where charged particles are trapped.[16] The trapped belts, composed principally of protons and electrons, are shown in simplified form in Figs. 3 and 4. Although ions of higher nuclear charge and mass are present, they contribute only a small risk to humans because of their relatively small concentrations. Potential sources of these trapped particles are the decay of albedo neutrons, i.e., those neutrons produced by GCR that interact with atmospheric constituents, or particles from the ionosphere or the solar wind. Mechanisms that transport these particles to the regions of trapping, and would accelerate them to energies of the trapped particles, have been proposed but not verified. Trapped particles can be lost through several mechanisms, including interaction with atmospheric constituents, adiabatic motions coupled with scattering and diffusion, and magnetic field disturbances during geomagnetic storms.

Figure 5 is a representative spectrum of protons in low-Earth orbit. Protons with energies between 20 to 400 MeV/nucleon are particularly significant in radiation protection. Figure 6 provides a simplified view of the trapped-electron belts for solar maximum and minimum. Figure 7 shows spectra of outer-belt electrons measured by Reagan et al.[17] Heckman and Nakano[18,19] have shown that the pitch-angle distribution of the trapped particles is Gaussian.

Variations in the Earth's magnetic dipole that affect the trapped belts have been discussed by Chapman and Bartels.[20] The largest source of such variations is related to the solar cycle. The intensity of solar ultraviolet radiation increases near solar maximum and heats up the Earth's atmosphere. This phenomenon increases the volume and density of the atmosphere at

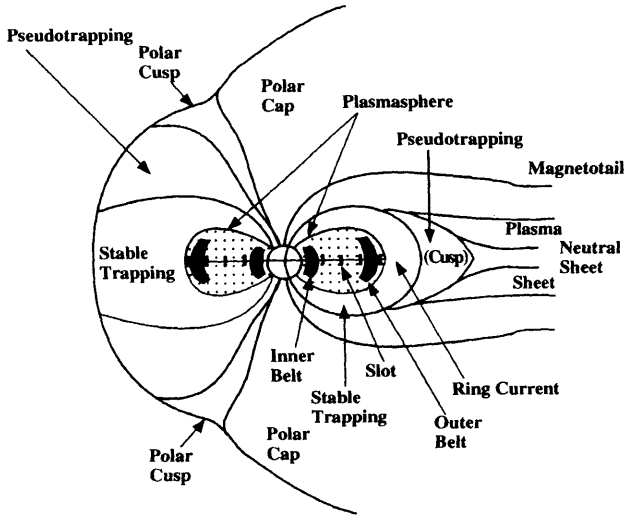

Fig. 2 Regions of Earth's magnetosphere where charged particles are trapped. From Ref. 16.

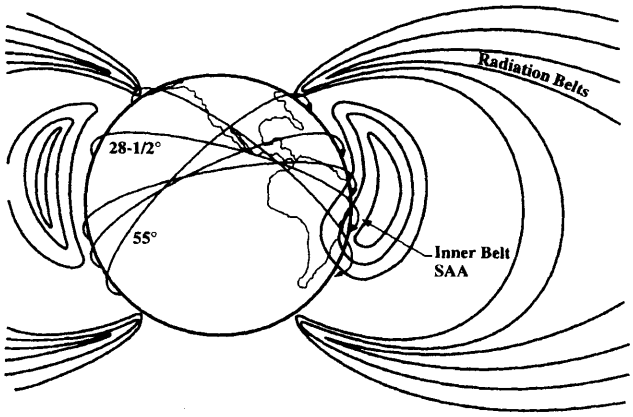

Fig. 3 Artist's conception of the trapped belts relative to Earth.

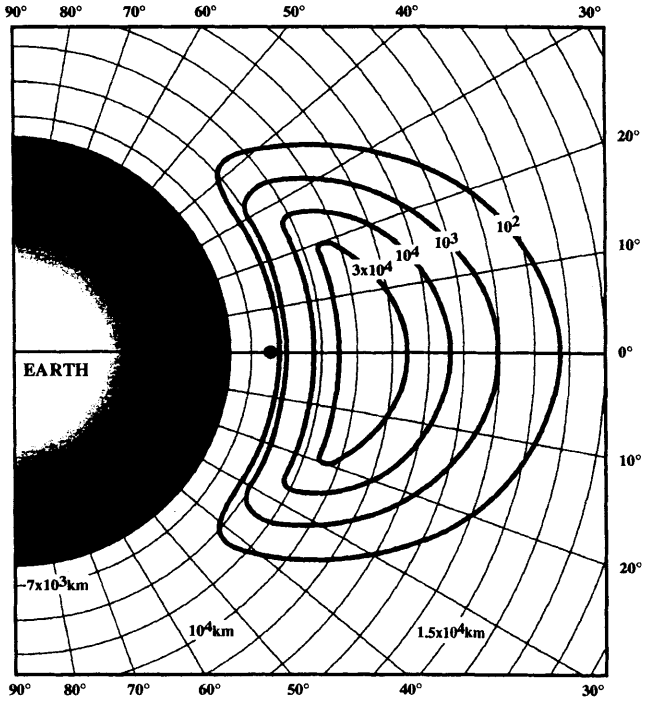

Fig. 4 Artist's conception of inner (proton) belt with approximated proton fluxes.

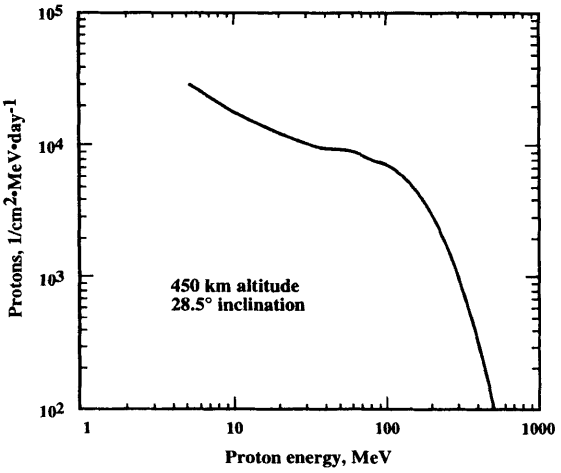

Fig. 5 Trapped-belt proton spectrum for orbit with 28.5° inclination, 450 km altitude.

higher altitudes, which in turn increases the rate at which trapped particles are lost.

Another variation in the trapped-radiation environment is related to a 0.27°/year decrease in the Earth's magnetic dipole. The dipole is not centered with the Earth's axis of rotation, but is offset by 489 km toward 20.4° N and 147.3° E. It also is tilted 11.1° with respect to the Earth's axis. This displacement moves the trapped belts downward in altitude over the South Atlantic near Brazil, a phenomenon known as the South Atlantic anomaly (SAA). The SAA is important for two reasons: It is the primary source of radiation exposure for space crews in low-Earth orbit, and it is a region of enhanced particle losses due to atmospheric scattering.

An east-west anisotropy of trapped-particle fluxes was predicted by Lenchek and Singer,[21] and was first measured by Heckman and Nakano.[18] At the bottom of a helical path of a trapped proton, it is traveling eastward; at the top of the helix, it is traveling westward. A satellite traveling east is struck on its trailing edge by particles traveling east, and vice versa for the leading edge. Particles traveling west are emerging from a region where the atmospheric density is greater (lower altitude), and thus a larger fraction is removed from orbit. The difference in the particle flux that strikes the leading and trailing edges of a spacecraft can be substantial. For example, Harmon et al.[22] found doses to be 2.5 times higher on the trailing edge of the Long-Duration Exposure Facility (LDEF) than those on the leading edge.

Temporary variations in the trapped-proton belt also can result from insertion of particles by solar-flare particle events. This phenomenon is not well understood, particularly for effects in low-Earth orbit. The presence of a potential "second" proton belt was first reported by McIlwain[23] on Explorer XV. McIlwain could not relate this observation to a solar particle event (SPE), but did show that the second belt did not result from the "Starfish" high-altitude nuclear test. The presence of the second proton belt was confirmed later by measurements made on the Relay I satellite. More than two decades later, Petrov et al.[24] reported the creation of a second belt at Mir altitudes during the large SPE in September and October 1989 from "Lyulin" dosimeter measurements. Lobakov et al.[25] reported measurements of particle enhancements from the same SPE using the Lyulin dosimeter and the "Ryabina" radiometer. Others have reported their existence[26] and decay[27] as well, the latter through the use of a tissue-equivalent proportional counter and a particle spectrometer on five Space Shuttle flights during an 18-month period.

The creation of this second belt was attributed to the injection of particles from an SPE that occurred on March 22, 1991. Measurements allowed the temporal and spatial movement of the second belt to be assessed. Comparisons with observations aboard the Mir and unmanned satellites revealed the e-folding time of the peak of the second proton belt to be 10 months. Proton populations in the second belt returned to values typical of quiescent periods within 18 months. The increase in absorbed dose attributed to protons in the second belt was approximately 20%.[27]

The most widely used models of trapped-belt radiation were developed and distributed by the National Space Science Data Center, NASA Goddard Space Flight Center, Greenbelt, Maryland. These models provide time-averaged fluxes of protons and electrons in the trapped and pseudotrapped regions as a function of energy, L-shell, and position along the field lines at solar maximum and solar minimum. However, they do not provide information on pitch-angle distributions. Uncertainties

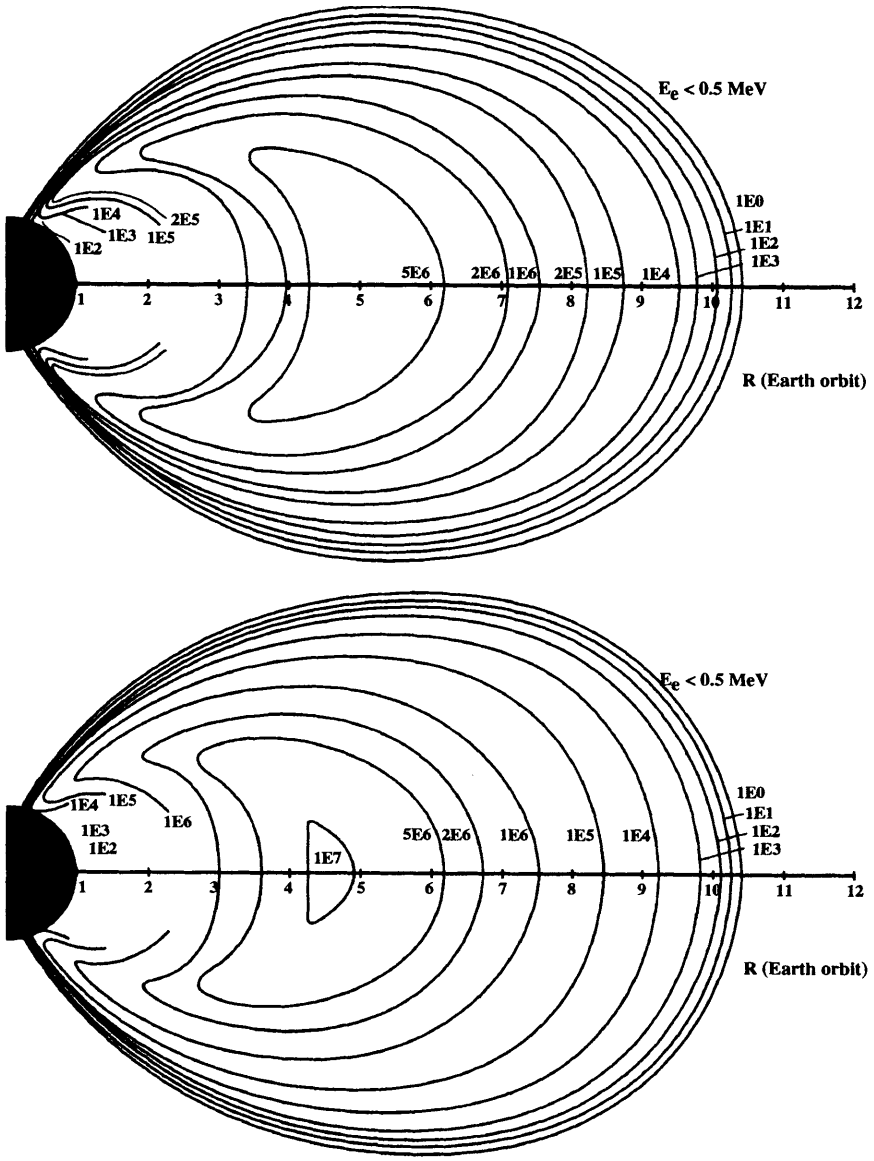

Fig. 6 Simplified view of the trapped electron belts for solar minimum (top) and solar maximum (bottom).

in integral particle fluxes from these models are estimated to be a factor of two at lower altitudes. Outer-electron belt fluxes, which are affected by magnetic storms, can vary by a factor of ten.

The NSSDC AP-8 proton model[28] was constructed from measurements made by 24 satellites over the period of July 1958 to June 1970. Proton integral spectra are given for the energy range from 0.1 to 400 MeV. Badhwar and Konradi[29] derived an energy-dependent distribution from omnidirectional fluxes at fixed B and L coordinates by using an inversion method. Figure 8 shows the spatial proton-intensity distribution as a function of these coordinates.

The NSSDC AE-8 electron model, an updated version of an earlier model,[30] gives trapped-electron fluxes for energies between 0.04 and 7.0 MeV. Measurements used to construct the AE-8 model were obtained from 23 satellites between August 1959 and April 1978. Diurnal variations of the electron belts at high altitudes and latitudes are described as a function of local time. Temporal, stochastic variations are described by a statistical model. Other time variations and belt dynamics also are described in the model documentation. Figure 9 shows the electron-density distribution for energies greater than 1 MeV vs B and L coordinates, and Fig. 10 shows the electron spectra at 400 km altitude and 28.5° inclination for solar maximum and minimum.

Other models have been developed for special applications. For example, a semi-empirical model of the trapped-belt environment was developed by Watts et al.[31] for use in estimating potential exposures for a space station. This model also includes the Heckman and Nakano[18,19] proton pitch-angle distributions.

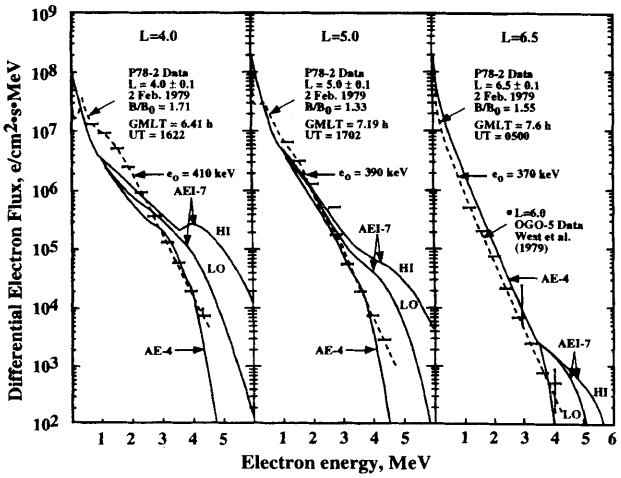

Fig. 7 Outer belt electron spectra. Adapted from Ref. 17.

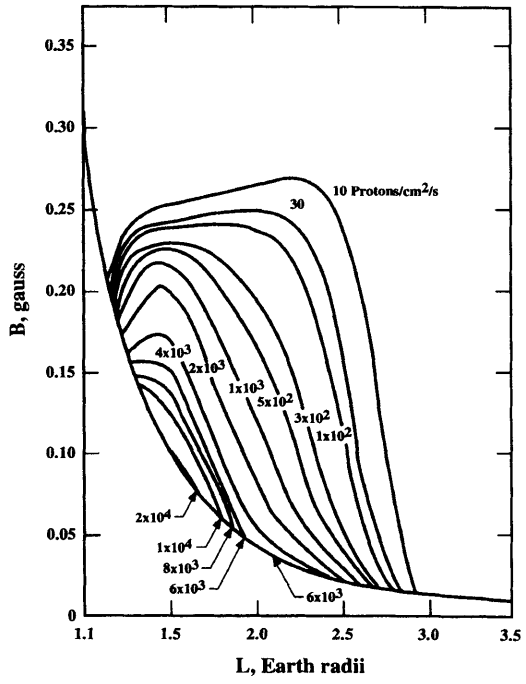

Fig. 8 Omnidirectional proton fluxes versus B and L (the McWallin parameter) for energies greater than 34 MeV. From Ref. 16.

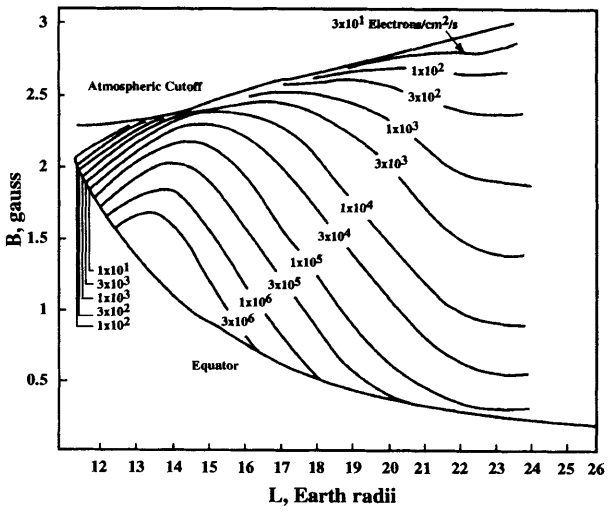

Fig. 9 Omnidirectional electron fluxes versus B and L (the McWallin parameter) for energies greater than 1 MeV for the October 1967 Epoch. From Ref. 16.

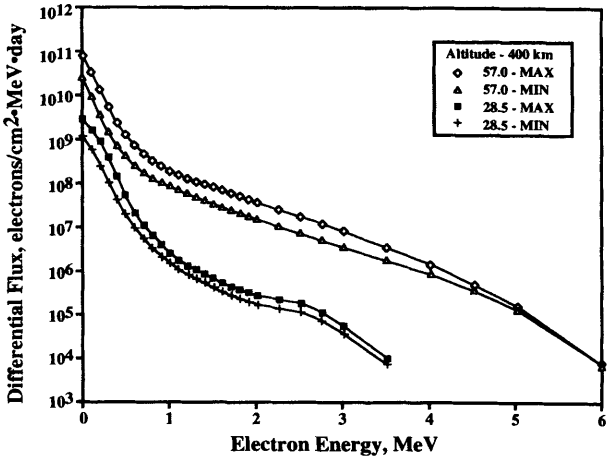

Fig. 10 Electron energy spectra at 400 km and 28.5° inclination for solar maximum and solar minimum.

Long-term changes in the Earth's magnetic field have substantially changed the location of the peak particle fluxes in the South Atlantic anomaly, which decreases the accuracy of the AP-8 model for that region. Figure 11 compares measurements made with the tissue-equivalent proportional counter in the SAA on the STS-37 Space Shuttle flight (April 1991) with AP-8-predicted proton intensity at a solar maximum that had occurred 22 years earlier.[26] The highest measured dose rate at 600 km in 1991 was located at –34.3° longitude; the model located it at –41.2°, indicating a 7° change over 22 years, an average of approximately 0.3°/year. Using a tissue-equivalent proportional counter on STS-28, Golightly et al.[32] obtained a rate of 0.32°/year for the westward drift of the SAA at 300 km. A northward drift of the maximum dose rate in the anomaly of approximately 0.16°/year also was suggested from these results.

Hardy et al.,[33] using thermoluminescent dosimeter measurements from Space Shuttle missions, evaluated the current applicability of the AP-8 model and concluded that it provides useful results for brief missions in low-Earth orbit. However, estimates for longer missions can involve substantial uncertainty, e.g., about 25% at Space Shuttle altitudes for solar minimum conditions.

In addition to differences in proton fluxes, Richmond et al.[34] found substantial changes in the proton spectrum when they used an inversion method on dose measurements obtained from Space Shuttle flight STS-51J. The peak of the measured differential proton-energy spectrum was found to be 30 MeV higher than that obtained from the AP-8 model.

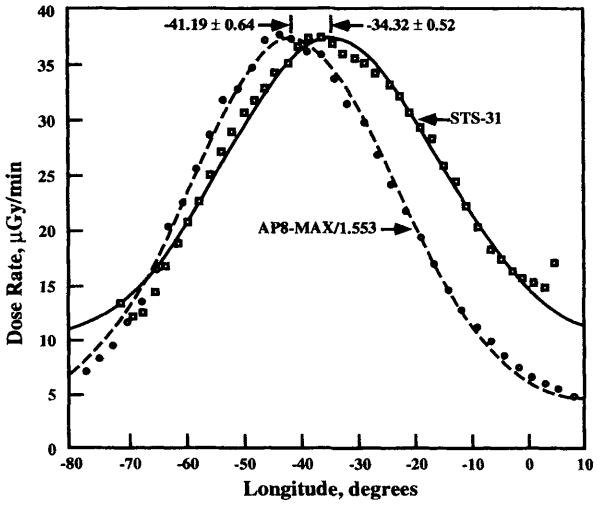

Fig. 11 Movement of the location of the maximum proton flux in the South Atlantic anomaly (SAA). Earlier data were from 1969. Average movement is approximately 0.3°/year.

Clearly, the trapped-belt proton model has significant errors attributable to temporal changes in the belts. New measurements and models are needed to ensure that mission doses are assessed accurately for future spaceflights. These new models should incorporate good spatial and temporal variations of the trapped-particle intensities related to the indices that cause those changes. In addition, descriptions of pitch-angle distributions should be included to allow estimation of directional doses inside the spacecraft. Several means of accounting for changes in the trapped-radiation environment have been proposed. One approach would be to update particle fluxes every 5 to 10 years with satellite measurements. A satellite in an equatorial orbit with an apogee of 8 R_E and a perigee of 1.1 R_E would be optimal, because this orbit would cross the full range of B and L values needed to reconstruct the proton belt configuration in the region where low-Earth-orbit human spaceflights will be conducted.

B. Galactic Cosmic Rays

Galactic cosmic rays (GCR) consist of energetic ions that originate within the galaxy but outside the solar system. Their intensities are modulated by solar-cycle changes in the interplanetary magnetic field. The greatest effects are observed for ions of the lowest energies. For example, intensities of ions with energies < 100 MeV/nucleon can vary by as much as a factor of 10, but those with energies > 10 GeV/nucleon typically vary less than 20%. The interplanetary magnetic-field strength increases as solar activity increases, and typically extends radially outward from the sun to a distance in excess of 70 AU. GCR entering the solar system are deflected by some degree by the more intense interplanetary magnetic fields, an effect that reduces GCR intensities in the inner heliosphere.

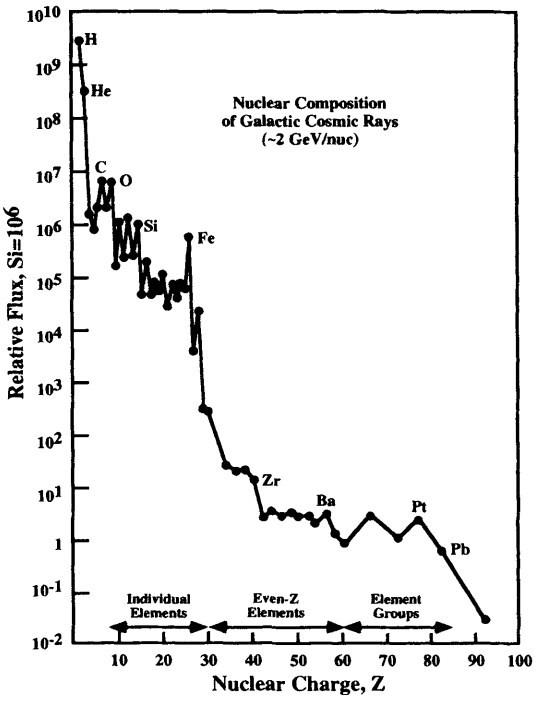

Fig. 12 Relative composition of galactic cosmic ray ions as a function of nuclear charge. From Ref. 41.

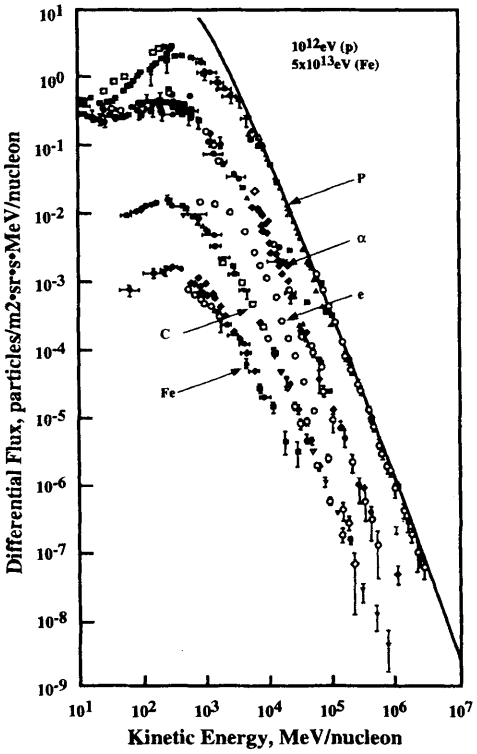

Fig. 13 Energy spectra for major galactic cosmic ray ions as a function of kinetic energy. The curve is the spectrum for interstellar space. Reproduced with permission from Ref. 36.

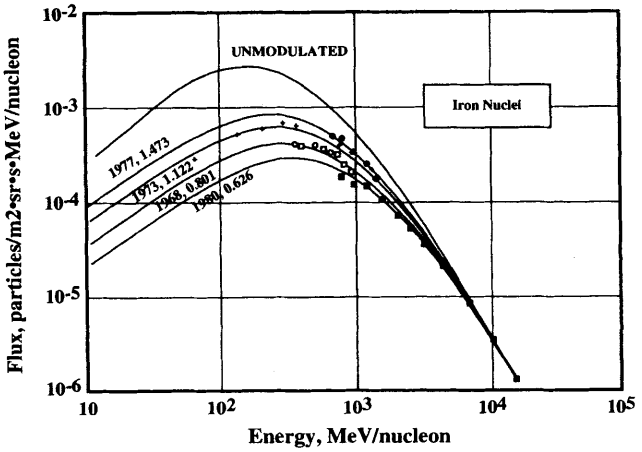

Fig. 14 Spectra of galactic cosmic ray iron ions at various periods of the solar cycle measured by several investigators. The curves are from the model of Badhwar and O'Neill (Ref. 37).

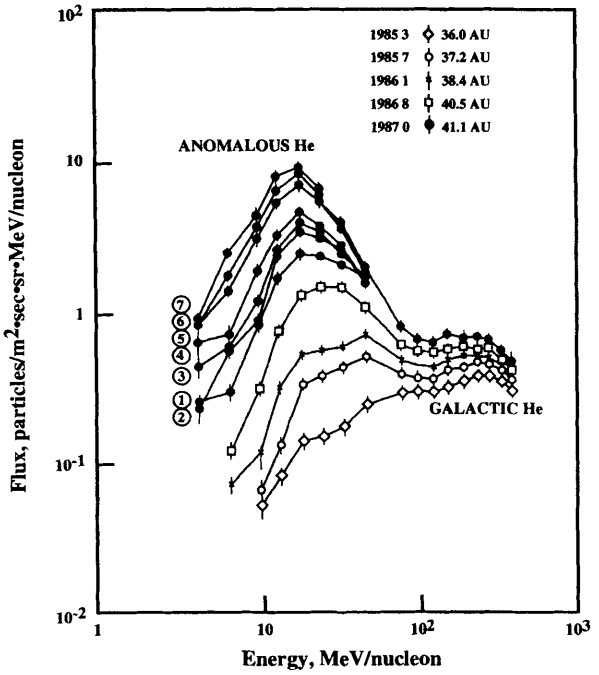

Fig. 15 The anomalous helium component of galactic cosmic rays shown for different parts of the solar cycle. From Ref. 42.

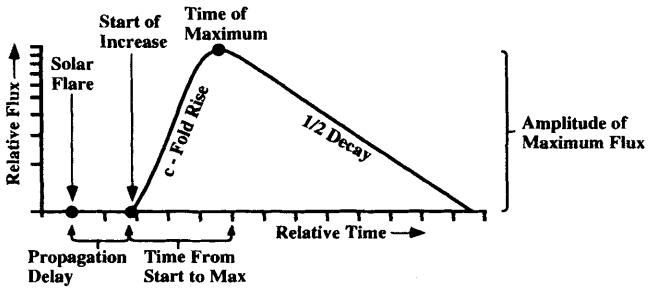

Fig. 16 General temporal characteristics of solar proton event flux at 1 AU. From Ref. 44.

GCR also are deflected by the Earth's magnetic field, which reduces their intensity inside the Earth's magnetosphere. Figure 12 shows the relative abundance of GCR ions in interplanetary space at solar minimum.[35] Figure 13 shows the energy distribution of the more abundant GCR.[36] The GCR spectrum extends to energies > 1 GeV/nucleon. Ions with such energies can penetrate a distance of 1 meter of water before being stopped. They have a mean free-path of about 10 g/cm^2 between nuclear interactions.

Badhwar and O'Neill[37] recently developed a GCR-solar modulation model that calculates the spectra of ions as a function of the solar cycle with a mean weighted root-mean-square (RMS) error of less than 10 percent.[38,39] In developing this model, GCR-ion spectra measurements were fit by using a solution of the time-independent, spherically symmetric Fokker-Planck equation. This particular solution accounts for the effects of diffusion, convection, and adiabatic deceleration. A parameter related to the diffusion constant was derived by using proton and helium data for the years 1954 to 1990 as a function of solar activity level. This parameter then was used to estimate the intensities of other ions, including iron. Figure 14 shows the spectrum of GCR-iron nuclei as a function of solar activity. Using this model, Adams et al.[40] found the highest GCR intensities ever recorded to be those during the 1977 solar minimum.

Measurements from several satellites show that GCR intensities vary with radial distance out to at least 47 AU from the sun. Mewaldt et al.[41] estimated the decrease to be 1 to 2% per AU for protons. An "anomalous" increase in the intensity of six ions (He, C, N, O, Ne, and Ar) has been observed as a function of the solar cycle. Figure 15 shows the variation of He ions over a solar cycle.[42] The anomalous component is produced when solar ultraviolet radiation ionizes neutral interstellar materials, and the resulting ions are accelerated inside the heliosphere. Only 5% of the He flux above 10 MeV/nucleon and 1% above 100 MeV/nucleon are contributed by the anomalous component. Their intensities decrease at about 15% per AU.

C. Solar Particle Events

Solar particle events (SPE) are a manifestation of solar flares, although not all solar flares accelerate charged particles that propagate out from the sun in the direction of the Earth. Figure 16 shows the typical time-intensity profile of an SPE.[43] The rise in intensity is related to the location on the sun at which the flare occurred and to the time needed for particles to propagate to the Earth. Particles originating in flares that are close to the "footprint" of the interplanetary magnetic field connecting to the Earth (Fig. 17) propagate more quickly.[44] The field lines that intersect Earth have a "footprint" at 57° west of central meridian. Rise times of particle intensities

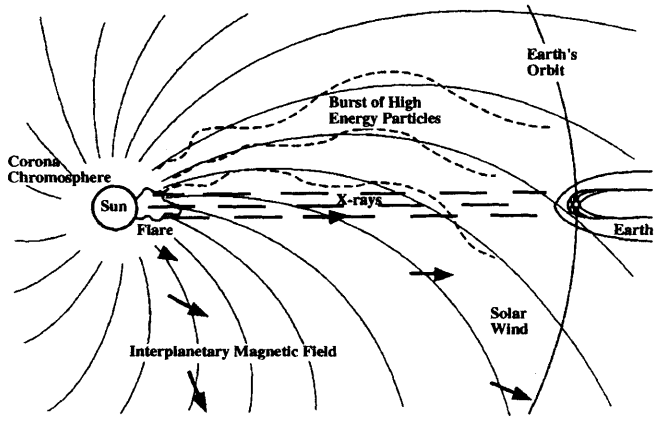

Fig. 17 Illustration of the gross features of the interplanetary magnetic field. From Ref. 44.

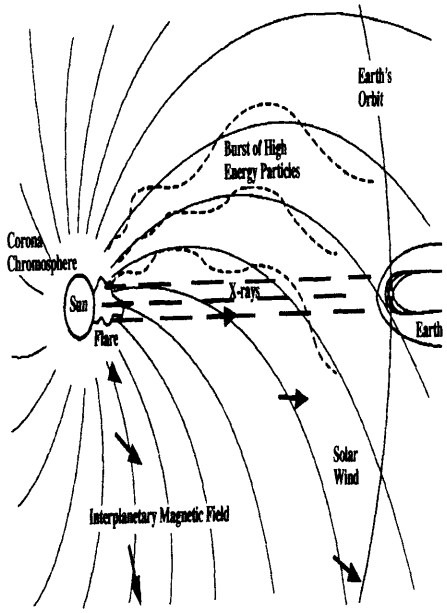

Fig. 18 Proton spectra of several of the largest solar particle events. Reproduced with permission from Ref. 45.

typically are longer for solar flares that occur in the eastern hemisphere.

The size of SPE can vary by many orders of magnitude. The location of the flare that produces the SPE is one factor that affects the size. The mean rise time of the six largest SPE in solar cycle 21 was 40 hours for particle energies > 10 MeV; the minimum rise time was 10.5 hours. The largest SPE ever measured, that of August 4, 1972, had a time-integrated intensity of 5×10^9 particles/cm^2 with energies > 30 MeV, and 1.1×10^{10} particles/cm^2 with energies > 10 MeV.

Energy spectra of SPE also vary considerably. Figure 18 shows the spectra of several large SPE.[45] In addition to protons and helium, ions with higher atomic charge have been observed in SPE. Their spectra are relatively soft and their

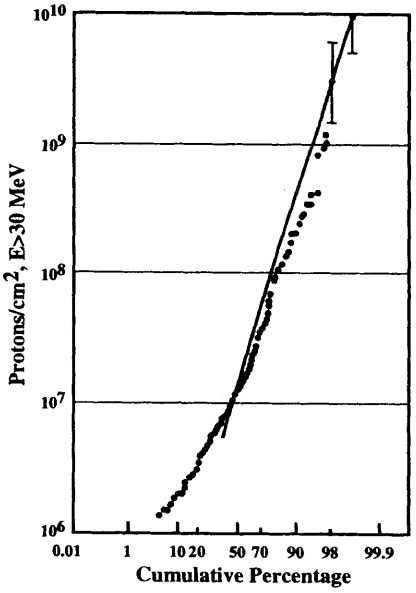

Fig. 19 Frequency distribution of solar particle event size for all events that occurred between 1956 and 1986. Distributions shown for event fluences > 10 and 30 MeV. Reproduced with permission from Ref. 46.

intensities significantly lower. Some SPE have protons with energies high enough to penetrate to the ground, where they (or their secondaries) can be detected. The largest event ever observed (via ground measurements) took place on February 23, 1956. This event produced particles with energies > 17 GeV.

Figure 19 shows the statistical distribution of SPE size based on measurements of 201 events between the years 1963 and 1985 for fluences between 10 and 30 MeV.[46] Fewer than 1% of the SPE had integrated fluxes > 10 MeV of > 10^{10} protons/cm^2.

In addition to flux, estimates of radiation danger must consider the energy spectrum of SPE. The distribution of particles with respect to energy E (or the equivalent value of magnetic rigidity) can be described in terms of power (e.g., E^{-7}) or an exponential law (e.g., $e^{-R/Ro}$). The characteristic rigidity of the spectrum R_o can vary from 10 to 300 MV. When R_o is small, much less shielding is needed to protect against dose effects. SPE are distributed randomly with regard to R_o, and can be described as follows[47]:

$$f(R_o) = \log_e / (\sqrt{2\pi\sigma^2 R_o}) \bullet e^{-(\log_e R_o - m_2^2/2\sigma_2^2)}$$

where $m_2 = 1.879$ and $\sigma_2 = 0.199$, according to results from the 19th and 20th solar-activity cycles.

Large SPE are more probable during the solar maximum years. Figure 20 shows all the large SPE from solar cycles 19, 20, and 21. These events occurred exclusively during the 4 years on either side of solar maximum,[46] which suggests that large SPE are not expected during the half of the solar cycle that brackets the solar minimum.

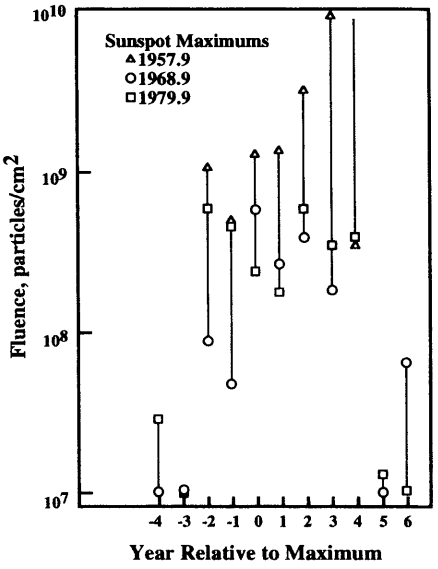

Fig. 20 Annual fluences from solar particle events between 1956 and 1986 relative to solar maximum (integral fluences greater than 10 MeV). Reproduced with permission from Ref. 46.

D. Geomagnetic Screening

The geomagnetic field in near-Earth orbit can provide some protection against SPE and GCR, and thus the dose of either SPE or GCR at a given point in that orbit should be calculated in terms of the magnitude of the geomagnetic threshold. The geomagnetic threshold is defined as the minimum energy of a particle passing from interplanetary space to a given point.[48] The coefficient of dose attenuation of the geomagnetic field æ is equal to the ratio of the dose in near-Earth orbit to the dose in interplanetary space measured at the period t behind the same shielding ϕ:

$$æ = K\int_0^T \phi(t)\left[\int_{E_{cutoff}}^{E_{max}} dF_x(E)/dE \bullet C(E)dE\,dt\right] /$$

$$K\int_0^T \phi(t)\left[\int_{E_{min}}^{E_{max}} dF_x(E)/dE \bullet C(E)dE\,dt\right]$$

where $F_x(E)$ is the spectrum behind the screening; C(E) is the conversion coefficient from flux to dose; $E_{cutoff(t)}$ is the geomagnetic threshold at a moment of time t; E_{max} and E_{min} are the upper and lower limits of the energy spectrum of SPE or GCR; and T is the duration of the SPE.[49]

The coefficient of dose attenuation is a function of the rigidity of the spectrum of cosmic rays, level of disturbance of the geomagnetic field, orbital inclination, and to a lesser extent, flight altitude. When Mir orbits in a quiet geomagnetic field, this coefficient varies from 10^{-4} for SPE with low characteristic hardness ($R_o \approx 40$ MV) to 10^{-2} (for $R_o > 150$ MV). During moderate and powerful geomagnetic disturbances, ae is not correlated with R_o and ranges from 1 to 0.5. Shielding thickness plays a larger role in "soft" SCR spectra and in quiet geomagnetic fields. For GCR and hard SPE, this function is significant only for orbits with low inclinations. The protective effect of the geomagnetic field in low-Earth orbit is the main factor responsible for protecting crews from radiation therein.

II. Passage of Space Radiation Through Matter

A. Energy Deposition

Ionizing radiation produces damage in living beings by depositing energy as it passes through tissue. It leaves an ionization trail with a narrow core of dense ionization and an outer penumbra of δ-rays (recoil electrons knocked out of orbit) that diffuse outward from the core. The damage produced by ionizing radiation in a medium is a result of the absorbed dose, i.e., the energy deposited per unit mass of the medium. The international (SI) unit for an absorbed dose is the Gray (Gy), which is equivalent to one joule per kilogram. The absorbed dose D is directly proportional to the fluence F(E) and the stopping power S(E), and is inversely proportional to the medium density ρ:

$$D = (1/\rho)\int_0^\infty dE\, S(E)\, F(E)$$

Stopping power is a measure of the average energy loss per unit track length. It typically is expressed in units of keV/mm, and depends on the nuclear charge, the energy of the radiation, and the properties of the medium through which it passes. The Bethe-Bloch approximation to the energy loss per unit path is

$$S = (4\pi N Z_\rho^{\,2} Z_t e^4/mv^2)\,[\ln(2mc^2h^2w_{max}/I_t) - 2\beta^2 - (2C/Z_t) - d]$$

where Z_ρ is the nuclear charge of the projectile, N is the number of target molecules per unit volume, Z_t is the number of electrons per target molecule, m is the electron mass, v is the projectile speed, $\beta = v/c$, c is the speed of light, C is the velocity-dependent shell correction term, I_t is the mean excitation energy of the medium, d is a density-correction term, $h = \gamma b$, $\gamma = (1 - b^2)^{-1/2}$, and W_{max}, the maximum energy transferred to an electron, is

$$W_{max} = 2mc^2h^2/[1 + 2(m_e/M)\sqrt{1+h^2} + (m_e/M)^2]$$

where m_e is the mass of an electron and M is the mass of the projectile.

Energetic ions also lose their energy through nuclear reactions in human tissue and spacecraft materials by elastic, inelastic, nonelastic, capture, and spallation processes. The daughter products are ions of a smaller atomic charge and neutrons.

B. Modeling the Transport of Radiation through Matter

The probability of receiving a particular dose from space radiation depends on both the radiation field and the duration of exposure. Both primary and secondary radiation contribute to the risk. The energy spectrum must be known if the absorbed dose at a specific point in the body is to be estimated. Energy spectra can be obtained by modeling the transport of primary radiation through the space-hardware systems and the human body, taking into account changes in their energy and composition as they ionize and otherwise interact with nuclei of the medium. In some cases, modeling the transport of secondary radiation may be needed as well to determine its energy deposition at the point of interest.

Wilson[50] derived an analytical solution to the transport of space radiation by assuming a straight-ahead approximation of Boltzmann's transport equation for the passage of primary space radiation through matter. He assumed that fragments of the target media produced by the occasional, violent nuclear interaction are negligible. Although these assumptions are accurate for particles of high-incident energies, fragments of the primary radiation produced in nuclear reactions must be considered because of the momentum they share with the primary particles. This straight-ahead approximation of the transport equation also can be used for fragmentation nuclei, since their energies also are high.

Sources of space radiation other than that in the trapped belts usually are isotropic, i.e., the flux is the same from all directions, although fluxes can be anisotropic in the early part of some SPE. The transport equation usually is solved for a monodirectional radiation that is incident upon a slab, because this condition is equivalent to solving the equation for isotropic radiation incident upon a spherical shield. The mass-shielding distribution must be determined at the dose point of interest. In practice, space surrounding the dose point of interest is divided into a large number of solid angles.

The straight-ahead approximation of the transport equation is

$$[(\partial/\partial x - \partial/\partial E) - S_j(E) + S_j E]\, F_j(x,E) = \Sigma_{k>j}\, m_{jk}(E) S_k(E) F_k(x,E)$$

where $F_j(x,E)$ is the flux of j-type ions with energy E at a point x in a slab of material, S_j is the macroscopic fragmentation cross-section for type j ions in the medium, $S_j(E)$ is the stopping power of j-type ions with energy E, and m_{jk} is the probability of a k-type ion producing a j-type fragmentation ion.

The biologically significant quantity in human tissue is the dose-equivalent, which can be calculated from solutions of the transport equation for $F_j(x,E)$ by using:

$$H(x) = \sum\nolimits_j \int_0^\infty dE\, S_j(E) F_j(x,E) Q_j(E)$$

where $Q_j(E)$ is the quality factor of a j-type ion of energy E, a quantity based on biological effects derived from experimentation as well as from expert judgements.

III. Measuring Space Radiation

Space radiation dosimetry differs from other branches of radiation physics in that the energies of radiation to be measured can extend over many decades, can include particles of many different species, and require measuring several parameters. A variety of techniques and instruments have been developed to measure absorbed dose, dose-equivalents, particle flux and fluence, lineal-energy transfer spectra, and linear-energy transfer (LET) spectra, as well as particle charge, mass, and energy distribution. Most of these parameters vary temporally as well as spatially. The detectors used in space-based dosimetry include, but are not limited to, thermoluminescent dosimeters, plastic nuclear-track detectors, tissue-equivalent ionization chambers and proportional counters, and particle spectrometers. Each system forms a separate subject, the principles and methodologies of which are described elsewhere; a short history of the development of radiation measurement systems in the U.S. space program can be found in Ref. 51. Brief descriptions of some of these techniques are presented below.

A. Dosimetry

Space radiation dosimetry can be classified as active or passive. Active systems have been defined historically as those dosimeters that can be read during flight or have their measurements sent to Earth by telemetry for near-real time processing. The key element of active dosimetry systems is the real-time or near-real time measurement and assessment of that measurement. Hence, simple pocket-type ionization chambers with optical viewing readouts are considered active dosimetry systems despite their needing no spacecraft power. Passive systems, in contrast, have been defined as systems that are read and analyzed after landing. Two of the passive systems used to measure space radiation, thermoluminescent dosimeters (TLD) and plastic nuclear-track detectors (PNTD), are discussed below.

Thermoluminescent dosimetry (TLD) techniques have been used to measure crew radiation exposures since the beginning of human spaceflight.[52] The physics of the thermoluminescent phenomenon is simple. Ionizing radiation excites free electrons and holes in the conduction band of a material. The free electrons either can recombine or be attracted to trapping centers within defects in the material lattice. Heating the material later can reexcite the electrons, which return to conduction bands. As the excited state decays, visible and ultraviolet light are emitted, the amounts of which are proportional to the amount of energy absorbed during irradiation.

The advantages of these detectors are their small size and the fact that they need no power. Thus, a stack of several TLD chips can be used as a single dosimeter. The most popular material for such detectors is LiF, although CaF_2 also has been used. The response of LiF, which has been measured as a function of LET for a variety of ions, agrees well with trap theory.[53,54]

However, TLDs show a great deal of variation in response between individual LiF dosimeters, as well as between different batches of dosimeters. Their response also depends on the devices' thermal and irradiation histories.[55] Thus, TLDs must be selected carefully both for uniformity of response and for deriving an empirical relationship of that response as a function of LET. Such analyses form the backbone of the Space Shuttle TLD system.[33,34,52] TLD systems are used in the Russian space program as well.[56] The biggest disadvantage of these devices is that they provide only the time-integrated physical (absorbed) dose. Thus, the dose cannot be separated into its components (e.g., GCR, SPE, or trapped radiation); no information on the LET distribution is available; the biological dose-equivalent cannot be obtained; and temporal distribution is not available. Despite these shortcomings, TLDs remain a most useful detection system. Moreover, recent advances in measuring a secondary (higher temperature) glow peak may allow rough estimates of absorbed doses from low- and high-LET particles.[57,58]

Price's and Walker's discoveries that fission fragments produce tracks in natural mica and other insulators, and that the visibility of the tracks can be enhanced by chemical etching,[59] greatly expanded the field of dosimetry. About 150 different materials are known to produce characteristic needle-shaped tracks when ionizing radiation passes through them.[60] Modern systems that exploit the etching technique have included plastics and polycarbonates—hence the name plastic nuclear-track detectors (PNTD). The three most popular materials currently used are cellulose nitrate, CR-39 (American Acrylics, Inc.), and Lexan®.

One important feature of track detectors is their ability to measure a portion of the LET spectrum. Although a detection threshold in the rate of ionization exists for primary radiation, the exact value of this threshold depends on the etching method, the plastic manufacturing process, and its exposure history. Thus, only the LET spectra above a given threshold can be studied. The response of PNTDs has been shown to be inconsistent with a dE/dx criterion that δ-rays with enough energy to produce tracks at longer distances from the core do not produce a site that the enchant can penetrate.[61] Fleischer et al.[62] proposed an ion-explosion spike model to explain the formation of these tracks. Katz and Kobeitch[63] proposed a δ-ray model, which stresses that only δ-rays within some fixed radial distance from the primary core contribute to track formation. Although the two models are quite different in approach, both predict that the quantity Z^2/β^2 (Z being the atomic charge of the plastic and β the fraction of speed of light of the particles) is more important than LET. The δ-ray model did account for the inactivation cross-section in various biological samples and plastic tissue analogs. Benton[64] applied the idea of restricted energy loss[65] to suggest that only moderately low energy δ-rays are important for track formation. Benton[66] used a collimated ^{90}Sr β-particle source to produce etchable tracks in cellulose nitrate, which supports the theory that δ-rays are responsible for track formation.

Thermosetting polymers, CR-39 in particular, have properties ideal for detecting the heavy-ion component of space radiation. They are relatively insensitive to the low-LET natural radiation background on the Earth's surface, thereby ensuring low background tracks. PNTD are typically etched by nonsolvents such as KOH or NaOH and are read microscopically.

The small mass and volume of these etch-track detectors make them particularly useful as personal dosimeters. Their inherent disadvantage is that they provide no temporal resolution. In addition, the number of tracks that develop depends strongly on the etching process (especially time and temperature). Also, a detector response depends on exposure orientation and can require large corrections or special calibrations. The minimum sensitivity of etch-track detectors currently in use is about 5 keV/μm, and thus more than 60% of the trapped-belt protons cannot be studied with them. Furthermore, data analysis of PNTD is extremely labor-intensive unless aided by sophisticated track-recognition instruments. The maximum fluence that can be detected and analyzed is limited by track overlap frequencies, and restricts the use of these detectors to a narrow range of very low doses.

B. LET-Spectrum Measurements: Microdosimetry

Active instruments are needed to provide time-resolution of radiation measurements during space missions. Of the large variety of such instruments, microdosimeters and particle spectrometers will be discussed in the following sections.

As mentioned previously, not all secondary δ-rays lead to damage in insulators. Because biological tissue sites are relatively small, the same is likely to be true for them. In addition, the stochastic nature of ionization loss becomes much more important. The principles of microdosimetry are based on measuring the energy deposition in tissue volumes of about a micron in diameter.[67–69] In terms of charged-particle energy loss, tissue volumes ranging from about 0.3 μm to several μm in diameter can be replicated by using gas at low pressure. Since the physical basis of the relative biological effectiveness (RBE) of different types of radiation is thought to result from differences in the spatial distribution of ionization along the track, physical quantities can be measured and related to biologically relevant quantities. Radiation protection experts now recommend that the quality factor be expressed in terms of LET, which can be measured directly by microdosimeters.

The most common microdosimetry detector, the tissue-equivalent proportional counter, consists of a small, nearly spherical tube filled with a low-pressure gas such as propane. A potential of 600 to 800 volts is applied to a wire that passes thorough the tube, producing a gas gain of approximately 200. Amplification can produce an overall sensitivity of 120 electrons (rms). Care must be taken in designing proportional counters in order to avoid contamination from the plastic used in the surrounding construction. Attention also must be given to the stability of the wire, vibration levels, and the location of preamplifiers to avoid microphonics. To minimize the requirement for large data storage or telemetry, lineal-energy loss measurements are grouped into semilogarithmic energy

bins, and the number of particles that deposit an amount of energy in each interval in the gas during a set time is counted. The gain of such devices has been demonstrated to be stable for more than a year, and calibration tests using ion beams at a particle accelerator have verified the ability of such instruments to measure LET distribution accurately.[70]

Since these instruments measure lineal-energy loss but not linear-energy transfer, mathematical transformations are needed. These transformations are a function of the chord-length probability distribution of particle ionization tracks in the counter tube. Spherical geometry allows accurate calculations of this distribution. Instruments using this technique have been flown on Space Shuttle and Mir.[37,71-73]

C. LET-Spectrum Measurements: Particle Spectrometry

Microdosimetry instruments cannot distinguish among particle types, nor can they provide information on the arrival direction of the particles. Detecting the arrival direction of GCR is not important since their fluence is isotropic. However, trapped-belt protons are highly directional and energy-dependent. Radiobiological studies indicate that inactivation or transformation cross-sections for cells are not a function of LET but rather of the nuclear charge Z and velocity β of a particle, where $\beta = v/c$ (velocity v is expressed in units of the velocity of light, c). The restricted energy-loss model predicts a dependence of these cross-sections on Z^2/β^2. Knowing the particle charge and velocity thus provides a means of computing the relevant energy loss parameter in any medium.

When a nonrelativistic particle of charge Z and velocity β comes to rest in a stack of detectors, the amount of energy that it deposits in a top thin layer of thickness Δx is

$$\Delta E \sim (Z^2/\beta^2)\Delta x$$

Figure 21 is a cutaway view of how detectors in a particle spectrometer can be stacked to allow discrimination of energies over a broad range. If the particle is stopped in the bottom detector, its residual kinetic energy E is

$$E = m\beta^2/2$$

and thus

$$E\Delta E \sim mZ^2$$

Every isotope can be represented by a unique hyperbola proportional to the mass of the particle and the square of its nuclear charge. Thus, measurement of ΔE and E yields a measure of the kinetic energy per nucleon, particle charge, and isotopic mass. Care must be taken with such detector systems to limit the acceptance angle of the spectrometer so that variations in the particle-path length are minimized. One option is to use position-sensitive detectors that can provide the arrival direction of the particle and avoid these path-length variations.

As particle energy increases, it becomes impractical to increase the depth of total E detectors because of possible interactions of the particle in the detector material. The charge, mass, or energy of these high-energy particles cannot be calculated. However, a different arrangement can be used that replaces the total E detector with a Cerenkov detector. The light output L, which can be measured with a photomultiplier tube, is

$$L = KZ^2 (1 - \beta_0^2/\beta^2)$$

where K is a constant and β_0 is the cutoff velocity below which no Cerenkov light is generated. β_0 is related to the real part of the index of refraction n by $\beta_0 = 1/n$. UV-transparent Cerenkov materials provide cut-off energies per nucleon as low as 180 MeV/nucleon for solids and up to several tens of a GeV/nucleon for gases. The charge and velocity of the particle can be determined from measurements of ΔE and L. Both the technique that measures $E\Delta E$ and the one that measures $L\Delta E$ can yield energies and nuclear charges of particles over a wide range. Although other techniques that provide velocity and mass information are available in the laboratory (e.g., time-of-flight, magnetic sector, etc.), these techniques are difficult to implement in space experiments because of size (geometry) and weight considerations.

IV. Biological Effects

A. Atomic and Molecular Effects of Ionizing Radiation in Tissue

The biological effects of radiation result from energy being deposited in living tissue.[74] Energy deposition, consisting mainly of ionizations and excitations of the atomic and molecular constituents of tissue, takes place very quickly, in periods comparable to the traversal time of the incident particles ($\sim 10^{-16}$ s). The original pattern of energy deposition behaves as if the energy were stored in a volatile chemical memory, consisting of all the chemical radicals and molecular products left over from the initial "physical" stage of energy deposition. The primary ionization tends to produce secondary energetic electrons that disperse through the material and produce ionization. Within approximately 10^{-12} s after the initial ionizations, electrons in polar liquids like water (the major constituent of tissue) are either captured ("solvated") or combine with other molecules to produce highly reactive chemical species (free radicals). These free radicals undergo further chemical reactions before they are inactivated (within about 10^{-6} s). The chemical reactants diffuse from their formation site, reacting with the medium, until the energy deposition pattern is "read" by biologically sensitive sites, mainly the deoxyribonucleic acid (DNA) molecules in cellular nuclei.

The effect of radiation at sensitive sites can be fixed, repaired, and modified by cellular mechanisms.[75] When the original lesion is not fully repaired, the transformed cell can

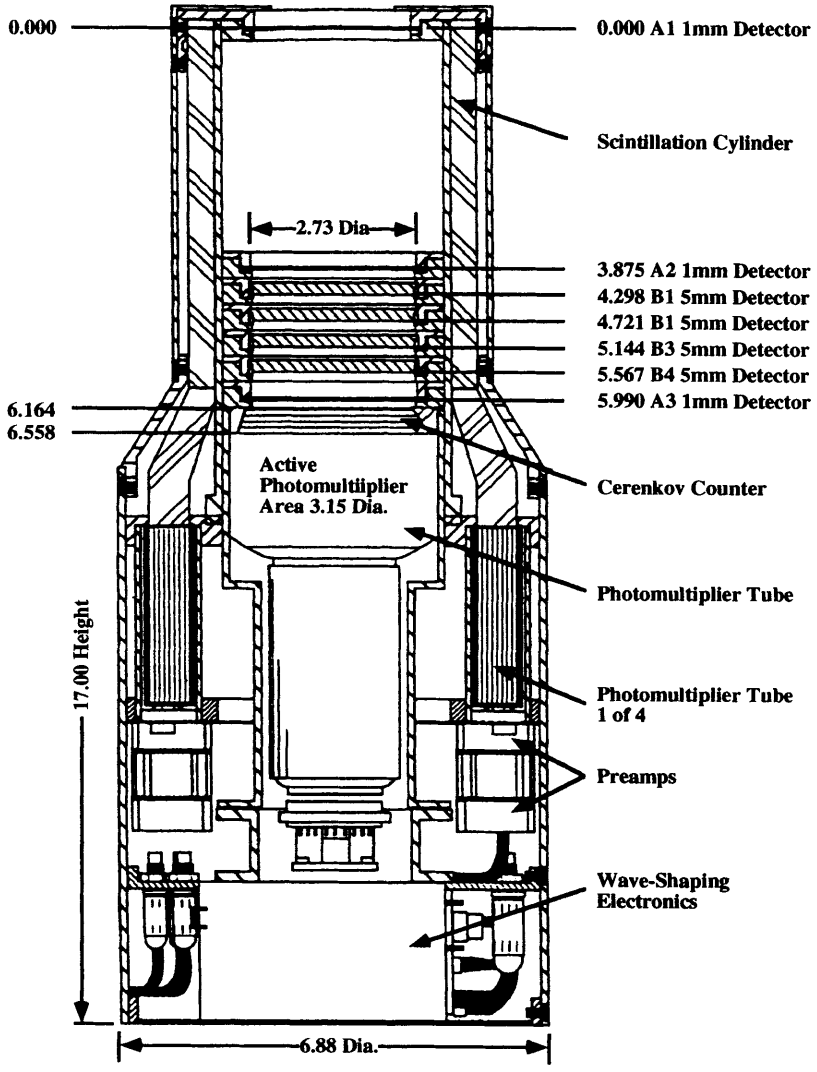

Fig. 21 Schematic of a particle spectrometer. Dia, diameter in cm.

die (or produce daughter cells that die after a finite number of divisions). If the cell does not die, it (or its progeny) can express its changed properties as further injury to the organs and tissues with which it interacts. The time scale associated with the biological manifestation of radiation damage is comparable to the time scale of biological processes, and can involve days or even years.

The basic unit of any living organism is the cell. The DNA molecules within the cellular nuclei contain the information required to synthesize intracellular proteins and cell reproduction. Other cellular structures participate in cellular function, but DNA is by far the most sensitive to radiation. The action of radiation on living cells therefore is considered on the basis of its interaction with DNA. When incident radiation deposits energy directly into the target DNA molecules, the process is referred to as a "direct" effect. Any modification of DNA by chemical intermediaries, principally the radiolysis of the surrounding water, is referred to as an "indirect" effect. Direct effects are of greater concern for heavy charged particles, whereas indirect effects are of concern for X-rays and similar radiation.

Molecules can be restored to their preirradiation condition through three mechanisms: recombination, restitution, and repair.[74] Recombination refers to ions or radicals coming together to form the molecule from which they originated. Restitution is the chemical restoration of altered molecules to their original state without the intervention of enzymatic or other biocatalytic steps. Repair is the restoration of molecular function produced by any of the catalytic processes taking place in the cell.

Strand breaks are the most important of the mechanisms resulting in initial damage to DNA. Single-strand breaks are repaired efficiently by intracellular mechanisms, but double-strand breaks are not, and are more likely to lead to cell death. Double-strand breaks can occur either as two neighboring single-strand breaks caused by direct action, or as the result

of interactions between two independent single-strand breaks separated by less than some as yet unknown critical distance.

Cell death is defined as the loss of reproductive ability, since seriously damaged cells often are able to function in some ways as long as the chemical sites involved in those functions are not themselves damaged by the radiation. Cell survival, e.g., the ability of cells to divide into colonies, is an end point best measured in the laboratory. In living organisms, cell death becomes manifest only when the function of an organ or tissue is impaired. Cell function can be modified by nonlethal changes in DNA that lead to neoplastic transformation, which is thought to be the first of a sequence of events leading to cancer. Further events, resulting from subsequent radiation or stimulation by so-called promoting substances, must take place before the cell can be considered "precancerous." Precancerous cells do not always lead to cancer; further changes in the cell and surrounding tissues are required for this so-called "promotion" stage. Even in the absence of cancer initiation, permanent changes in cellular DNA may occur as mutations. Such mutations, when they occur in reproductive cells, can be inherited and manifested in the progeny of the irradiated organism. These changes in a cell that has maintained reproductive integrity are known as "genetic effects."

The effects of radiation can be measured in terms of the number of colonies formed by surviving cells, number of cells manifesting a measured change, probability of tumor formation, or other indicators. Other factors being equal, the effects of radiation are a function of the absorbed dose for a given type of radiation. However, different types of radiation do not necessarily produce the same observed effect at the same observed dose, since the microscopic distribution of deposited energy and the chemical processes deriving from it are not the same, even though the average energy deposition (absorbed dose) may be the same. The differences in biological action for different types of radiation at the same absorbed dose are known as the "quality" of the radiation.[76]

For historical reasons, x-rays have been used as the standard reference against which all other radiation types have been compared. In the field of radiation protection, the dose-equivalent H has been used to normalize biological damage to that of x-rays by means of the relationship

$$H = QD$$

where Q is the mean quality factor over lineal energy. For radiation protection purposes, the quality factor Q is defined as a function of LET_∞ instead of being defined as a function of lineal energy. In addition, linear-energy transfer is used with no restriction on the maximum energy that the secondary electrons produce (i.e., the quantity used is numerically equal to the stopping power). The unit of dose-equivalent is the Sievert (Sv), where 1 Sv is assumed to have the same biological consequences as 1 Gy of x-rays.

Revised recommendations for radiation protection generated by the International Commission on Radiological Protection (ICRP)[77] are the basis of many current national regulations.[78] The latest recommendations define a new quantity, closely related to dose-equivalent, called the equivalent dose ($H_{T,R}$), which is related to dose by

$$H_{T,R} = W_R \cdot D_{T,R}$$

where $D_{T,R}$ is the average absorbed dose from radiation R in the tissue or organ T and W_R is the radiation weighting factor, which replaces the concept of quality factor and has been defined by the ICRP for different radiation types. However, the recommissioned Scientific Committee 75 of the NCRP recommends that a more accurate procedure with which to calculate space radiation exposures is to continue using the dose-equivalent defined by the ICRP,[78] but to use the ICRP[77] relationship between quality factor and LET (S. B. Curtis, private communication, 1992). This method is considered more accurate because some of the weighting factors defined by the ICRP for heavy-ion radiation[77] are thought to be incorrect.

Low-LET radiation (i.e., radiation from x-ray and gamma-ray sources) is often distinguished from high-LET radiation [i.e., radiation from high-energy heavy-ion (HZE) particles]. The electrons released in tissue by x-rays have mean LET values of 2–3 keV/μm; gamma rays have mean LET values in the range of 0.2 to 0.5 keV/μm. Radiation associated with LET values of 3.5 keV/μm or less are referred to as low-LET, and radiation with higher LET values is called high-LET. However, even low-LET gamma-ray sources may produce secondary electrons with high-LET values of 10–30 keV/μm.[74] In comparison, high-LET radiation produced by HZE particles can deposit up to a thousand times more energy per unit track length than low-LET radiation. Also, low-LET secondary electrons can pass through the space between DNA strands (~3 nm) without interacting with it; in contrast, some high-LET ions can produce an ionization trail so large that it inactivates nearly every cell it traverses.

Secondary electrons, as well as charged particles, do not lose energy continuously, but rather at discrete interaction sites; the distance between these sites depends on the density (and the chemical state) of the material. The distance between energy-loss interactions can be several microns for light particles like electrons and protons at high energies where the energy loss is minimal. Consequently, the statistics of energy loss will show large fluctuations, especially in very thin targets. Heavier particles in relatively dense materials like tissue will lose energy at a sufficiently high rate that a continuous slowing-down approximation to the energy loss is valid.

Neutrons, which have no charge, can penetrate relatively large distances without interacting with the medium, since they lose their energy only by interacting with the nuclei of the medium. When they do interact, the cascade of secondary ions that is produced can deposit large amounts of energy locally. For this reason, neutrons are regarded as high-LET radiation. In fact, neutrons have been the main source of high-LET radiation studied to date. On the basis of recent data on the maximum RBE values for cancer induction by intermediate-energy neutrons, the ICRP revised the definition of Q(L)

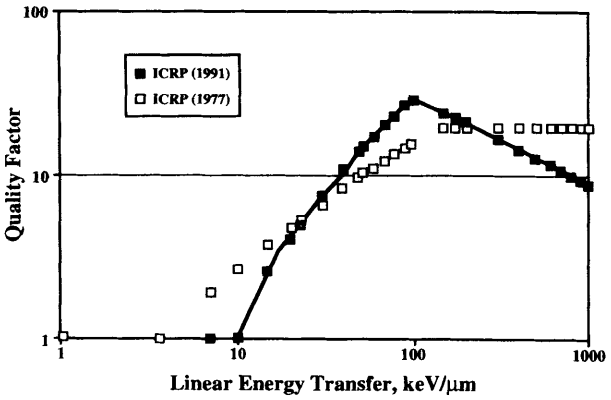

Fig. 22 Quality factor versus linear energy transfer (LET) for the latest recommended relationship (Ref. 77) and the prior relationship (Ref. 78). Reproduced with permission.

to the LET-dependence of Q[77,78] (Fig. 22). This revised definition recognizes the lesser effectiveness of heavy ions with LET greater than 100 keV/μm, presumably because of saturation effects or recombination.

B. General Health Effects: Early Effects of Acute Exposures

Health effects from exposure to space radiation usually are considered in two categories, early (acute) effects and late (delayed) effects. Early effects are manifested within hours, days, or weeks after high-dose whole-body exposure, e.g., that delivered by an SPE. Late or delayed effects usually appear months or years after exposure and include tissue damage, impaired fertility, lens opacification, cancer induction, heritable effects, and developmental abnormalities. Of these delayed effects, attention typically is focused on cancer induction. Crews will be exposed unavoidably to low-dose-rate GCR and also may be exposed to higher dose-rate particles from SPE.[79]

The acute effects of ionizing (but low-LET) radiation on humans at dose levels above 100 rem (1 Sv) are reasonably well understood; effects typical of whole-body exposures to these levels are described in Table 1. The acute effects of high-LET radiation are not as well known with respect to dose, but qualitatively can be expected to be the same as low-LET radiation.

Exposing humans to doses greater than 50 rem (0.5 Sv) produces characteristic symptoms known collectively as "radiation sickness." The onset, duration, and severity of these symptoms depend on the dose. Typical symptoms may include headache, dizziness, malaise, abnormal sensations of taste and smell, nausea, vomiting, diarrhea, decreased blood pressure, decreased white blood cells and platelets, increased irritability, and insomnia. In humans, three organ systems are most important in the acute radiation syndrome. The central nervous system is most affected by exposures in the thousands of rem (tens of Sv); the gastrointestinal system is most sensitive to exposures between 550 and 2000 rem (5.5 to 20 Sv); and the hematopoietic system is most sensitive to 550 rem (5.5 Sv) or less.

Effects of whole-body exposures to low doses of 50 rem (0.5 Sv) or less usually are mild, and occur only during the first day after exposure. Blood cell counts may drop slightly, but survival of the individual is almost certain. As the exposure range rises to 100 to 200 rem (1.0 to 2.0 Sv), prodromal effects increase in severity. At 200 rem (2.0 Sv), the incidence of vomiting increases to 70%; fatigue and weakness is evident in approximately 30–60% of those exposed.[79] Significant destruction of bone-marrow stem cells may lead to a 25–35% drop in blood-cell production. As a result, mild bleeding, fever, and infection may occur during the fourth and fifth weeks after exposure.

At dose-equivalent exposures of 200–350 rem (2.0 to 3.5 Sv), prodromal symptoms begin earlier and affect a greater number of exposed persons. Moderate diarrhea 4 to 8 hours after exposure is experienced by 10% of the population. Most victims tire easily and experience mild to moderate weakness intermittently over a 6-week period. Under normal conditions, vomiting and diarrhea are not enough to cause serious fluid loss or electrolyte imbalance. However, in hot or humid conditions, the combined fluid loss and electrolyte imbalance could become serious. Injury to the hematopoietic system is manifested by moderate bleeding, fever, infection, and ulceration 3 to 5 weeks after exposure in more than half of those exposed. During the fourth and fifth weeks, diarrhea may complicate the condition.

Most individuals exposed to 350–550 rem (3.5 to 5.5 Sv) experience severe prodromal symptoms. Severe, prolonged vomiting can affect electrolyte balance. Most exposed individuals show moderate to severe fatigue and weakness for many weeks. If untreated, 50–90% of those exposed will die from extensive injury to the hematopoietic system, as manifested by overwhelming infections and bleeding during the third to sixth weeks. Nausea, vomiting, and anorexia may recur, and approximately half will experience diarrhea, electrolyte imbalance, and headache. Terminal conditions may be complicated by dizziness, disorientation, fainting, prostration, and symptoms of infection.

Severe nausea and vomiting on the first day after exposure will be experienced by almost all those exposed to 550–750 rem (5.5 to 7.5 Sv), with dizziness and disorientation accompanying these symptoms. Bone-marrow stem cells and granulocytes are almost completely eliminated, leaving untreated persons susceptible to overwhelming infections, including those from their own injured gastrointestinal tract. The combination of hematopoietic and gastrointestinal damage reduces the survival of all untreated persons to two to three weeks. Moderate to severe bleeding, headaches, hypotension, dehydration, electrolyte imbalance, and fainting are common.

Exposure to dose-equivalents of 750–1000 rem (7.5 to 10.0 Sv) reduces the survival time for untreated persons to about 2.5 weeks. Symptoms resemble those in the preceding range, except that severe nausea and vomiting may continue into the third day; hypotension affects 80% and moderate fever 30 to

Table 1 Expected short-term effects in humans from acute whole-body radiation (Ref. 79)

Dose (rem)[a]	Probable Physiological Effects
10–50	No obvious effects, except minor blood changes.
50–100	Five to ten percent experience nausea and vomiting for about 1 day. Fatigue, but no serious disability. Transient reduction in lymphocytes and neutrophils. No deaths anticipated.
100–200	Twenty-five to fifty percent experience nausea and vomiting for about 1 day, followed by other symptoms of radiation sickness; 50 percent reduction in lymphocytes and neutrophils. No deaths anticipated.
200–350	Most experience nausea and vomiting on the first day, followed by other symptoms of radiation sickness, e.g., loss of appetite, diarrhea, minor hemorrhage. Up to 75 percent reduction in all circulating blood elements. Death of 5-50 percent of those exposed.
350–550	Nearly all experience nausea and vomiting on the first day, followed by other symptoms of radiation sickness, e.g., fever, hemorrhage, diarrhea, emaciation. Death of 50 to 90 percent within 6 weeks; survivors convalesce for about 6 months.
550–750	All experience nausea and vomiting within 4 hours, followed by severe symptoms of radiation sickness. Death of up to 100 percent.
750–1000	Severe nausea and vomiting may continue into the third day. Survival time reduced to less than 2.5 weeks.
1000–2000	Nausea and vomiting within 1-2 hours. All die within two weeks.
4500	Incapacitation within hours. All die within 1 week.

[a]100 rem = 1 Sv

45% during the first day; electrolyte imbalance persists from the sixth hour on; all have moderate to severe headache during the first day; and nearly 75% are prostrate before the end of the first week. Exposures to 1000–2000 rem (10 to 20 Sv) cause severe nausea and vomiting within 30 minutes of exposure, and symptoms continue intermittently until death in the second week. A single, acute whole-body exposure of 4500 rem (45 Sv) can cause death as early as 32 hours after exposure,[80] and all exposed will die within one week.

Studies of Japanese atomic-bomb survivors have provided the most complete database on the health effects of low-LET radiation in humans. A total of 75,991 people survived Hiroshima and Nagasaki, of whom 41,719 received doses greater than 0.005 Gy. Those who received smaller doses serve as an excellent control group. Data from these individuals are periodically updated and analyzed by the United Nations Scientific Committee on the Effects of Atomic Radiation (UNSCEAR) and the National Academy of Sciences' National Research Council Committee on the Biological Effects of Ionizing Radiation (BEIR). The most recent epidemiological data[81,82] are known as BEIR V. Results from these studies indicate that humans are less sensitive to the genetic effects of radiation than was previously thought. In addition, genetic effects in the offspring of atomic-bomb survivors, aging, and shortened lifespan were found to be insignificant. However, the incidence of hard tumors is significantly greater than had been indicated by earlier data; indeed, the chief late effect in atomic bomb survivors is cancer[83] (Fig. 23). Examination of the DS86 dosimetry data indicates that neutrons did not contribute significantly to total doses, but rather most of the dose was contributed by gamma rays (low-LET radiation). However, these results have been questioned recently because the possible contribution of "fast" neutrons was not considered in the DS86 dosimetry.

C. General Health Effects: Late Effects

Humans who are exposured to radiation levels that are not acutely lethal usually seem to recover from the initial syndrome within a month or two. However, their incidence of mutations, cataracts, and certain tumors is greater than that of control populations. The genetic effects of radiation are manifested by increased frequency of mutation; however, as noted above, genetic effects have not been demonstrated unequivocally in the descendants of atomic-bomb survivors. The threshold for cataract development seems to be several hundred rem of acute exposure to low-LET radiation; lower doses do not produce clinically significant damage. Carcinogenic

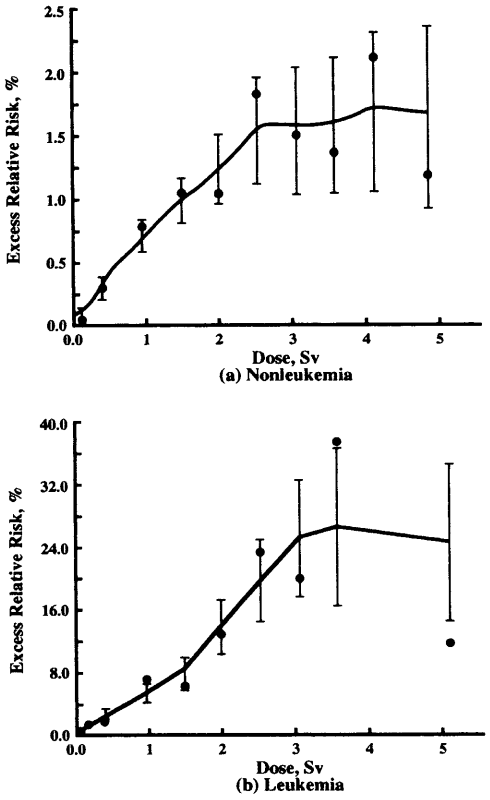

Fig. 23 Dose response curves (a) for all cancers except leukemia and (b) for leukemia. The points are excess relative risk in 0.5 Sv intervals. Reproduced with permission from Ref. 83.

effects, the focus of most concern in assessing radiation risks, are discussed in the following paragraphs.

The ability of radiation to induce tumors was first noted 10 years after the discovery of x-rays, when medical workers were found to have an increased incidence of cancer. Extensive experimental results and clinical observations accumulated since that time have shown that radiation, in sufficient quantities, can cause neoplasms in virtually all organs. The type of tumor that forms depends on the area irradiated, the dose and quality of the radiation, and the genetic background, age, and sex of the recipient. Skin and bone tumors appear most frequently after local irradiation; other solid tumors and leukemia generally result from whole-body irradiation. Moreover, irradiation can speed the expression of preexisting neoplasms as well as increase the absolute incidence of types of cancer.

The incidence of myelocytic leukemia and cancer of the breast, lung, thyroid, and bowel are known to increase after exposure to high doses and high dose rates of low-LET radiation. The latency period, the length of time between exposure and cancer appearance, varies from about 5 years for leukemia to more than 27 years for cancers of the pharynx and larynx, and also varies greatly among individuals. The mean latency of leukemia in atomic-bomb survivors was 14 years (range 5 to 20 years); median latency for all other types of cancer was about 25 years.

The overall risk estimate for radiation-induced leukemia, obtained from atomic-bomb survivors at Hiroshima and Nagasaki, is 46 deaths per million people exposed per rem (per 0.01 Sv). By comparison, the total cancer risk has been estimated at 70–165 deaths per million people per rem per year, depending on the risk-projection model.[84] Insufficient data preclude estimating the effects of dose rate on cancer induction in humans.

Many of the higher LET-types of radiation in the space environment (e.g., protons and heavy ions) have kinetic energy sufficient to penetrate both the normal shielding of the spacecraft and the human body. Very few data have been obtained for heavy ion radiation, and essentially no radioepidemiologic data exist for human cancer resulting from exposure to protons and high-LET heavy particles. The biological effects of such particles currently are extrapolated from experiments with animal models (e.g., mouse Harderian gland, rat skin, rat mammary gland) and cultured mammalian cells.[79] In general, high-LET radiation is more effective than photons in inducing tumors at low doses. The low-dose-rate effects of high-LET radiation on tumor induction are complex and may be specific to the tissues affected. However, the dose rate of high-LET radiation seems to have much less of an effect on cancer induction than the dose rate of gamma rays.[79] An understanding of the physical characteristics of the radiation and the biological nature of the tissue of interest is necessary in order to interpret the effects of fractionation and protraction of both low- and high-LET radiation.

V. Exposures of Space Crews

A. Trapped Belt Radiation: Low-Earth Orbit

The U.S. Long-Duration Exposure Facility (LDEF) was exposed to space radiation in low-Earth orbit for 69 months, having been placed in a 28.5° inclination orbit by the U.S. Space Shuttle mission STS-41C (at 528 km) in April 1984 and retrieved (at 333 km altitude) by STS-32 in January 1990. Figure 24 illustrates results from Atwell's calculations of the proton and electron contributions to the dose received by the LDEF using the environments provided by the AP-8 and AE-8 models. As shown in that figure, trapped-belt protons are the dominant source of dose for shielding thicker than about 0.3 g/cm^2. Figure 25 shows the daily dose-equivalent to the blood-forming organs as a function of shielding thickness for a 28.5° inclination orbit at two altitudes (463 km and 556 km).

Skylab was placed in a 50° inclination orbit at an altitude of 435 km in July 1972. It was visited on three flights by crews of three astronauts each between mid 1973 and early 1974. Table 2 lists the mean exposures to each crew as measured by thermoluminescent dosimeters. The dose rates for Skylab 4 are among the highest to which U.S. astronauts have been exposed.

Figure 26 illustrates the relationship between skin dose (measured by TLDs worn by crew members during flight) and spacecraft altitude for Space Shuttle flights[33] that varied

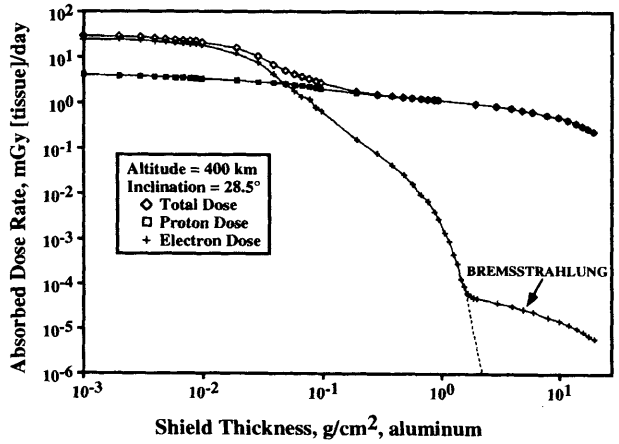

Fig. 24 Relative contributions to the total dose from trapped protons and electrons.

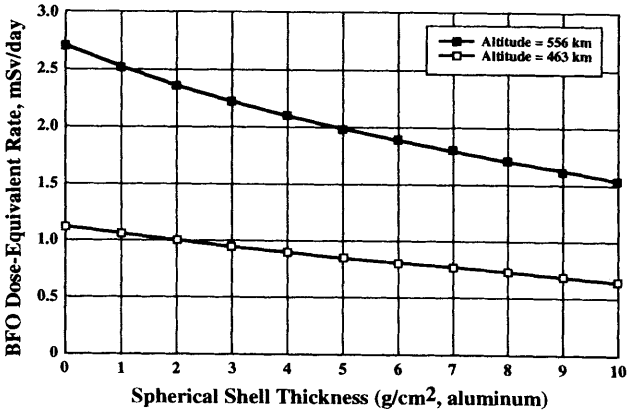

Fig. 25 Dose-equivalent for the blood-forming organs (BFO) versus shielding thickness calculated for 28.5° inclination orbit at altitudes of 463 km and 556 km.

from 2 to 15 days in duration, had altitudes between 215 and 617 km, and orbital inclinations between 28.5° and 62°. For comparison, the Mir space station has a 51.5° inclination orbit and a mean altitude of 350 km. Nguyen et al.[71] measured doses on Mir during the Soviet-French Aragatz mission between December 1988 and April 1989 by using a low-pressure tissue-equivalent proportional counter. The mean daily dose and dose-equivalent rates during December 1988 were 0.322 mGy/day and 0.617 mSv/day, respectively. Between March and April 1989, the mean daily dose and dose-equivalent measured rates were 0.451 mGy/day and 0.799 mSv/day, respectively. The mean quality factor obtained from these data was 1.9±0.3. The maximum dose rates on Mir were observed during passes through the South Atlantic anomaly, where the dose rates and dose-equivalent rates were 0.755 mGy/h and 1.050 mSv/h, respectively. The mean quality factor computed from the anomaly measurements was approximately 1.4.[71]

Some of the neutrons produced by GCR ions interacting with atmospheric nuclei are scattered back into spacecraft orbital altitudes. Secondary neutrons also are produced by GCR and trapped-belt protons interacting with spacecraft materials.

Table 2 Mean doses and dose rates measured on the three Skylab flights

Mission	Duration, days	Mission dose, mGy	Daily dose, mGy/day
Skylab 2	28	15.96	0.54±0.3
Skylab 3	59	38.35	0.65±0.5
Skylab 4	90	77.40	0.86±0.9

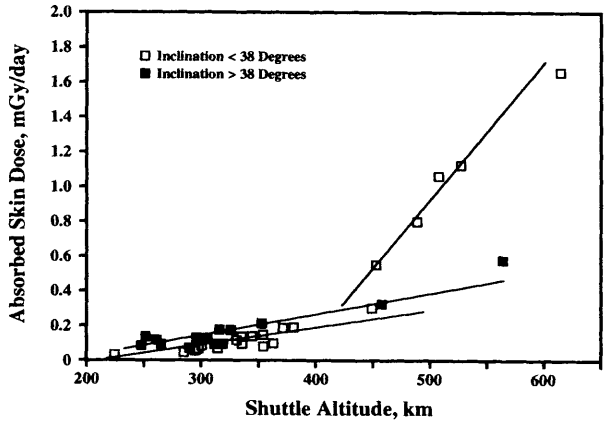

Fig. 26 Daily skin dose rates measured on Space Shuttle flights versus altitude and inclination. Straight lines are for viewing perspective only. From Ref. 33.

Neutron fluences, doses, and energy spectra have been measured occasionally during flights. Keith and colleagues[85-87] used activation foils with plastic spheres of different diameters to measure neutrons on Space Shuttle flights (Table 3). The neutron quality factor used was 20. At 300 and 600 km, the proton dose-equivalent rates were 2.5 and 14 times greater than the neutron dose-equivalent. For comparison, a bubble detector used on Mir measured a neutron dose-equivalent rate of 0.023 mSv/day.[71] Thus, Mir measurements are reasonably consistent with those made on Space Shuttle flights.

LET spectra provide insight into the contribution of high-LET radiation. Petrov et al.[88] measured integral LET spectra inside the Soviet Soyuz spacecraft on flights between 1958 and 1970 by using nuclear emulsions; the quality factor computed from these measurements varied between 1.2 and 1.4. Benton and Parnell[56] measured LET spectra on several U.S. and Soviet missions both inside and outside the Earth's magnetosphere by using emulsions, plastic track detectors, and electronic spectrometers. Since the detectors were behind shielding of different thicknesses, direct comparisons of these results are not meaningful. In addition, the typical 5 keV/μm threshold response of PTND means that a large percentage of the dose contribution from protons in the South Atlantic anomaly presumably was lost.

LET spectra have been measured inside the U.S. Space Shuttle on several missions by using a tissue-equivalent

Table 3 Neutron and proton dose-equivalent rates inside the Space Shuttle for flights with 28.5° inclination (Ref. 86)

Mission	Duration, days	Altitude, km	Proton equivalent dose rate, mSv/day	Neutron equivalent dose rate, mSv/day
STS-4	7.0	297	0.54	0.22
STS-5	5.1	297	0.043	0.023
STS-6	5.0	284	0.048	0.013
STS-31	5.0	617	1.66	0.188

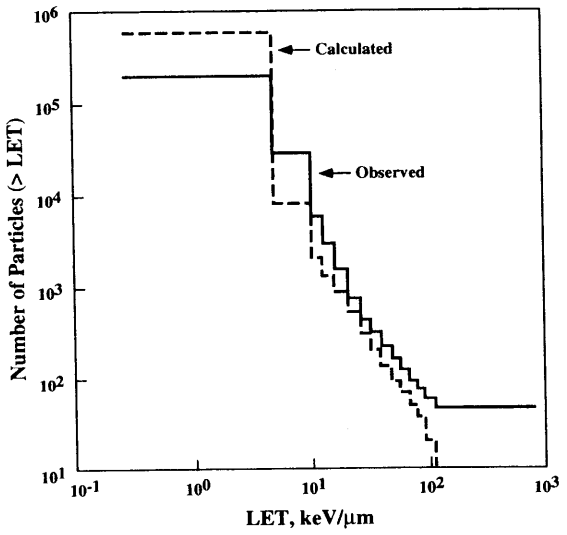

Fig. 27 Integral LET spectrum from trapped-belt particles measured on Shuttle flight STS-40 using a tissue-equivalent proportional counter. The calculated spectrum is from the AP-8 model (Ref. 89).

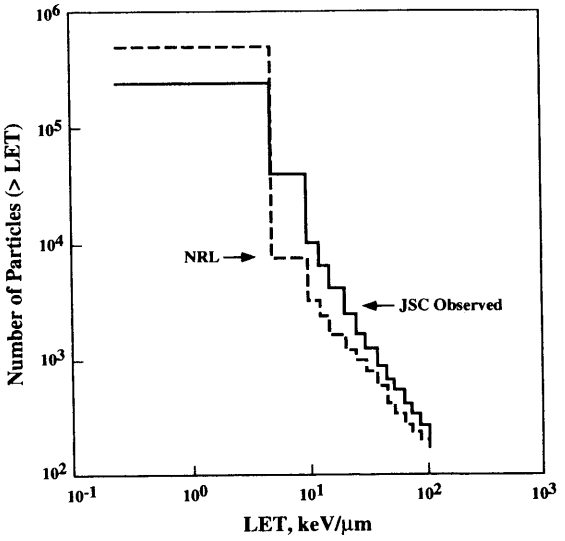

Fig. 28 Integral LET spectrum from galactic cosmic rays measured on Shuttle flight STS-40 using a tissue-equivalent proportional counter (Ref. 89). The spectrum labeled NRL was calculated using the model of Adams (Ref. 92). The spectrum labeled JSC was calculated from the model of Badhwar and O'Neill (Ref. 37).

proportional counter.[26,72,89-91] These instruments allow the contributions from trapped-belt ions and GCR to be separated, because the proportional counter is an active instrument that provides temporal resolution, and because trapped-belt and GCR are dominant at different portions of the orbit. An LET spectrum of trapped-belt protons measured on Shuttle mission STS-40 is shown in Fig. 27, in which an LET spectrum calculated from the AP-8 model environment is shown for comparison. The calculated spectrum is a factor of 3 greater than the measured spectrum below 5 keV/μm. In higher-energy channels, the measured spectrum is up to a factor of 5 greater. These differences are attributed to errors in the AP-8 model.

The GCR-LET spectrum measured on the same flight is shown in Fig. 28; the NRL spectrum was calculated from the CREME model of Adams,[92] and the JSC spectrum was calculated from Badhwar's and O'Neill's model.[38] For energies less than 5 keV/μm, both calculated spectra are greater than the observed spectrum. Between 5 and 100 keV/μm, the observed spectrum is greater than either of the calculated spectra. These differences decrease as LET increases, and probably result from inaccuracies in the model used to describe the transport of GCR through the Earth's magnetic field to the low altitudes of the Space Shuttle orbit.

B. Galactic Cosmic Rays

The GCR ions that contribute to most of the dose from space radiation exposures are iron (Fe), hydrogen (H), oxygen (O), silicon (Si), magnesium (Mg), helium (He), carbon (C), and neon (Ne). The important energy range is between 0.02 and 20 GeV/nucleon. For shielding as thick as the mean free path of a heavy GCR ion (10 g/cm^2), these 8 ions contribute about 80% of the dose-equivalent.[93,94] Half of the dose-equivalent behind a shield of that thickness is contributed by ions having energies greater than 0.85 GeV/nucleon. Nuclear fragmentation becomes an important consideration when shield thicknesses exceed one mean free path.

Badhwar et al.[5] calculated dose-equivalent rates from GCR as a function of shielding thickness for the "worst-case" 1977 solar-minimum spectra (Fig. 29). These results differ signifi-

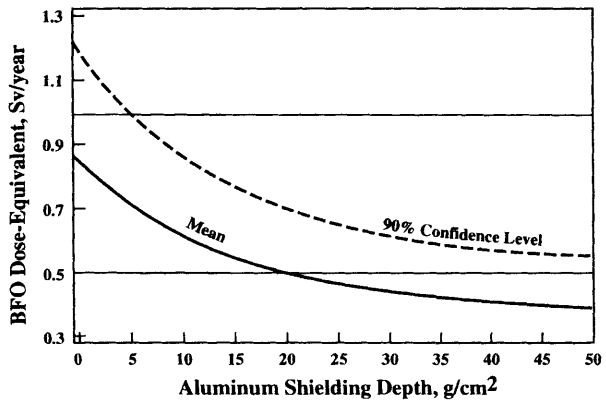

Fig. 29 Blood-forming-organ dose-equivalent versus shielding thickness for galactic cosmic rays. Intensities are from the model of Badhwar and O'Neill (Ref. 37) and the quality factor relationships from ICRP-60 (Ref. 77). They correspond to intensities of the 1977 "worst case" solar minimum (Ref. 40). The upper bound 90% confidence level dose-equivalent curve uses the uncertainty in GCR intensities of Badhwar and O'Neill (Ref. 37).

cantly from earlier estimates[95] that used the CREME model[92] for GCR intensities. The mean dose-equivalent calculated with the new estimate exceeds 0.5 Sv for an aluminum shield < 20 g/cm^2 thick. The uncertainty of the CREME model results is about 30%.

Curtis and Letaw[96] calculated the percentage of cells in a 100 mm^2 area that would be hit by GCR in free space during a year. They assumed that cells were at a depth of 5 g/cm^2 in a 30 g/cm^2 water phantom placed at the center of a 4 g/cm^2 spherical aluminum shell. Their calculations included the contribution of GCR-ion fragmentation. According to these calculations, more than 60% of the cells would be hit by one GCR ion of nuclear charge between 3 and 28, and 15% would be hit twice by ions in that charge range. Hence, the heavy-ion component of the space radiation environment clearly is significant in terms of biological damage and the resulting radiation effects.

C. Solar Particle Events

Figure 30 (Ref. 97) shows the free-space dose-equivalent to the skin, ocular lens, and bone marrow calculated for the August 4, 1972 SPE as a function of aluminum-shielding thickness. As illustrated, at least 6.3 g/cm^2 of shielding would be needed to reduce the dose-equivalent to the blood-forming organs to less than 0.5 Sv, and the skin dose-equivalent to less than 3.5 Sv. By comparison, 20 g/cm^2 shielding would reduce the dose-equivalent to the blood-forming organs to 0.05 Sv, to the skin to 0.16 Sv, and to the ocular lens to 0.15 Sv.

A group of SPE of sizes comparable to that of the August 1972 event took place in October 1989. The August 1972 event had a higher integrated flux (> 100 MeV), but the October 1989 spectrum was harder. Figure 31 illustrates the hourly mean proton fluxes that were greater than 30 MeV and 100 MeV during the October 1989 SPE. The SPE group was actually a superimposition of three separate events that took place within five days.

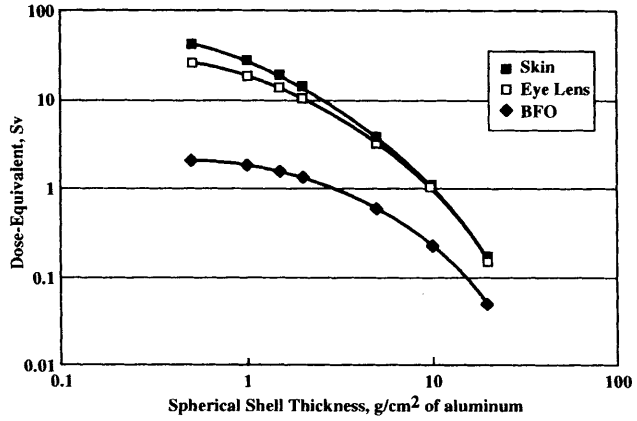

Fig. 30 Dose-equivalent for skin, eye lens, and blood forming organ versus thickness for the August 1972 solar particle event. Reproduced with permission from Ref. 97.

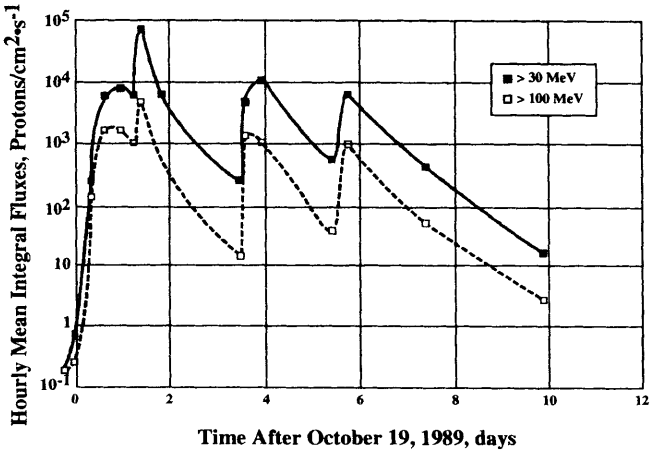

Fig. 31 Hourly mean proton fluxes for the October 1989 solar particle event group. Reproduced with permission from Ref. 94.

(The skin dose-equivalent rate never exceeded 0.1 Sv/h behind a shielding thickness of more than 5 g/cm^2.)

Measurements were taken aboard Mir with P-16 and IPD-2 dosimeters during these SPE (Table 4).[98] The maximum proton flux, with high energy E_r = 39–83 MeV, was recorded on October 20, 1989 at 16:00 UT on satellite GEOS-7. Moreover, this sharp increase in energy took place during a powerful geomagnetic disturbance, reducing the efficacy of geomagnetic screening by 1.5–2 orders of magnitude. For this reason, dose rate increased sharply to 0.2 Gy/h between 13:48 and 13:50 UT, and the cosmonauts sought refuge in the most protected area of the station, taking the IPD-2 dosimeter with them.

VI. Assessing Risks from Exposure to Space Radiation

A. Defining Risk

A risk estimate is the probability that a specified health effect is caused by exposure to ionizing radiation. The con-

Table 4 SPE doses measured aboard Mir with the IPD-2 and P-16 dosimeters during September and October 1989

Date	IPD-2 Dosimeter Dose, cGy	IPD-2 Dosimeter DE, cSv	P-16 Dosimeter Dose, cGy	P-16 Dosimeter DE, cSv
29 Sept 89	—	—	0.48	0.67
19 Oct 89	0.77	1.08	2.63	3.68
22 Oct 89	0.08	0.11	0.30	0.42
24 Oct 89	0.05	0.07	0.14	0.20
Totals	*0.90*	*1.26*	*3.55*	*4.97*

DE, dose-equivalent

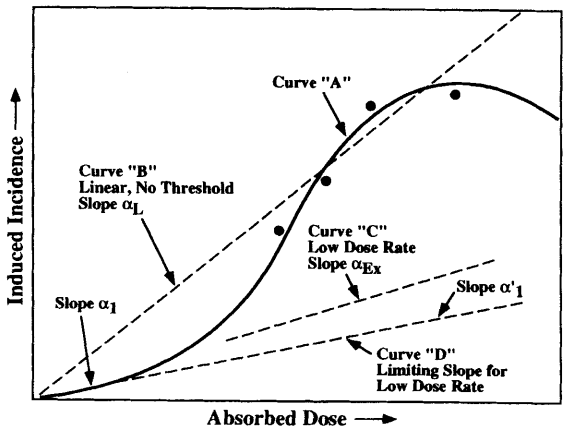

Fig. 32 Dose-response curves are based on various fits to the observed data. The solid line curve "A" is taken to be the true curve for high dose rate, high absorbed doses. Curve "B" is a linear fit to the four data points and the origin assuming there is no threshold. Slope $\alpha 1$ applies to the linear portion of curve "A." Curve "D" is assumed to be the "limiting slope for low dose rate." The dashed curve "C," with a slope α_{Ex}, is assumed to apply to low dose rates. Reproduced with permission from Ref. 99.

cept of risk from exposure to ionizing radiation, as postulated by the ICRP,[78] assumes that the probability of stochastic effects is directly proportional to the dose-equivalent. The probability of an effect is the product of two conditional probabilities, first that a person will be exposed to a given dose-equivalent, and second that the dose-equivalent will produce that particular effect. Thus, the risk consists of both a physical and a biological component.

B. The Dose-Response Curve

The relationship that describes the induced incidence of an effect as a function of dose is called the dose-response curve. Figure 32 illustrates the importance of choosing the appropriate analytical fit to the curve. Often, only a few data points at high doses are available with which to estimate the risk of incidence at low doses. For example, the best data on the effects of low-LET radiation on humans are those from the atomic-bomb survivors. However, the dose those people received was from a one-time, high-level, acute exposure. The risk of cancer from lower doses can be estimated only by extrapolating from these data, which obviously introduces uncertainties.

One approach often used is to obtain an upper-limit estimate from a "straight-line fit" (curve B) to data on an effect. The slope of the linear fit implies that the effect is independent of dose, but is related to the risk coefficient, which is taken to be linear at low doses because the response is assumed to arise from a single event. However, several observations suggest that the dose-response curve is curvilinear (curve A) rather than being a straight line. For example, repair mechanisms can affect the curve at low doses, and saturation of cell death can affect it at high doses. When two or more events are required to produce the response, the risk is proportional to the square of the dose-equivalent. A single, high-LET ion can cause a lesion, but two events involving low-LET radiation generally are thought to be required. The "low-dose" curve (curve C) of Fig. 32 is the slope of the dose response based on high-dose data extended to low dose rates. Curve D, the slope of the dose-response curve, defines the limiting slope at low dose rates.

C. Low-LET Radiation Risks

The severity of a biological effect from low-LET radiation, and perhaps high-LET radiation as well, depends on the rate of exposure. Risk models are based primarily on acute, high-dose exposure data that are extrapolated to continuous, low-dose rate exposures. As a consequence, the National Council on Radiation Protection and Measurements introduced a dose-rate effectiveness factor (DREF).[99] A DREF of 2 is recommended by UNSCEAR,[81] ICRP,[77] and NAS/NRC.[82] This factor should be applied for total absorbed doses less than 0.2 Gy regardless of dose rate, and for cumulative doses greater than 0.2 Gy when the dose rate is < 0.1 Gy/h. In almost all circumstances, the dose rates in space will be less than 0.1 Gy/h, and thus can be considered low-dose-rate exposures.

Applying the DREF of 2 to the most recent data from atomic-bomb survivors yields a nominal risk of fatal cancer in a working population (18 to 65 years of age) of 4% per Sv. This estimate assumes a linear extrapolation to low doses. (For comparison, the normal death rate from cancer of all causes in the general population is 19.3%.)

D. High-LET Radiation Risks

The carcinogenic and mutagenic effects produced by space radiation in humans are virtually unknown; thus, risk estimates for space travelers are based on data from human exposures to gamma and neutron radiation, and a few experiments with animals and cells exposed to heavy-ion beams from particle accelerators. Much research is needed in order to reduce the uncertainties in estimating the risk to humans exposed to heavy-ion space radiation.

Grahn's concept[100] of microlesions arose from the assumption that a single heavy ion will produce a "track" in tissue with a central zone of dead cells surrounded by mutated cells. The observation that a single ion traversing several cells damages the central core by the primary particle, and the penumbra by δ-rays, seems to support this concept; however, it has not been supported by experimental evidence.[10]

Quantitative data on the carcinogenic effects of heavy ions are available from animal and cellular studies. The mouse Harderian gland has been used extensively to assess carcinogenesis from heavy ions. Radiogenic Harderian-gland tumors are not lethal, and have no counterpart in humans. Nonetheless, this model system offers the advantages of having a low incidence of spontaneous tumors, and thus allows low-dose studies to be conducted with relatively small numbers of animals. This model, involving tumors of epithelial-cell origin, also allows tumor formation to be assessed with or without hormonal promotion. Argon and iron beams have RBE values of about 30 for inducing Harderian-gland tumors; heavy ions of lower LET have lower RBE values.[101] Curtis et al.[102] proposed a fluence-based risk coefficient that becomes constant at LET values greater than 200 keV/μm. Two other animal systems, rat mammary gland[103] and rat skin,[104] also have been used to study heavy-ion carcinogenesis. Neon ions were found to have RBE in the 2 to 4 range[10] for inducing mammary-gland cancer in the rat; the RBE for electron beams and argon ions in skin-tumor induction varied with dose, ranging from about 2 for low doses to 10 at high doses.[105]

These results indicate that RBE differs in different species and tissues, and much more information is needed to assess the risk of inducing lethal tumors (e.g., lung, mammary, and colon cancer) by heavy ions. Since many physiological and environmental factors, in addition to genetic damage, can influence cancer formation in animals, the carcinogenic effects of space radiation must be studied at the cellular and molecular levels if the mechanisms of carcinogenesis are to be understood in vivo. Experiments with cultured mammalian cells have generated both RBE values for heavy ions and information on the cellular and molecular mechanisms of radiation carcinogenesis. Similar results have been obtained on the relationship between RBE and LET in several cell systems.

The cell system most often used to study neoplastic transformation is the mouse embryonic-fibroblast line C3H10T1/2. Although these cells are nontumorigenic, a small percentage of exposed cells cultured for several weeks will lose their normal density-inhibition properties and become tumorigenic when injected into a syngeneic mouse. The tumors that form from these transformed cells can be lethal to the animal. Studies with this cell system have shown that RBE increases with LET up to 100–200 keV/μm and decreases at higher LET.[106] Similar results have been obtained with golden hamster embryo cells.[107] Hei and Hall[108] also showed that, for a given dose, the transformation frequency of C3H10T1/2 cells irradiated with protons, deuterons, and ^{3}He ions increases with increasing LET. Earlier studies with cultured Syrian hamster cells suggest that high-LET argon ions were as effective as 430 keV neutrons in causing neoplastic transformations.[109]

Despite the importance of knowing the carcinogenic effects of the low dose rates of high-LET radiation present in space, only limited information exists on the low-dose-rate effects of heavy ions. One study that suggested that low dose rates of high-LET heavy ions could enhance cell transformation[110] also found the magnitude of enhancement to depend on LET and to be less than 50%. Other investigators have reported enhancement factors greater than 2 for fractionated doses and low-dose-rate neutrons.[111,112] Thus, the effect of low dose rates seems to depend on the quality of the radiation.[113] The issue of whether low dose rates enhance transformation has become more complicated since Crompton et al.[114] noted an inverse dose-rate effect for somatic mutation in Chinese hamster cells irradiated by gamma rays.

Several investigators have tried to transform human cells in vitro to aid assessments of health risks from high-LET heavy ions. Human fibroblasts can be transformed by a single dose of x-rays[115] as well as by fractionated doses of gamma rays.[116] Ionizing radiation also can cause neoplastic transformation of human hybrid cells (Hela-x-skin fibroblasts).[117] X-rays and heavy ions can induce transformation in human epithelial cells[118,119]; interestingly, more than one exposure was needed to transform cells from normal to tumorigenic, even for iron particles. This indicates that several "hits" may be necessary for neoplastic transformation by ionizing radiation. This observation has significant implications for radiation risk assessments and warrants further study.

Overall, the data available on the carcinogenic effects of space radiation are far too few to allow health risks to be assessed. The greatest gaps lie in the low-dose-rate effects of low- and high-LET radiation, the response of human epithelial cells, tumor induction by heavy ions in important tissues (such as lung, breast, and colon), and the mechanisms of carcinogenesis by heavy particles.

E. Managing Radiation Risks

The risks to humans from space radiation can be managed in several ways. The goal of risk management is to prevent deterministic effects and to reduce the probability of stochastic effects to their minimum level. This latter philosophy, known as ALARA (as low as reasonably achievable), allows further risk reductions to be weighed against gains. At one time, dose limits were considered to be the upper limits of safe levels of exposure. This assumed that a threshold existed beyond which further exposure became unacceptable. The philosophy of ALARA, as discussed in ICRP,[78] considers a dose limit to be a lower level above which further exposure is totally unacceptable. In other words, it is not sufficient to reduce the exposure to values below the dose limit; rather, the goal is to limit the risk by making all exposures as-low-as-reasonably-achievable.

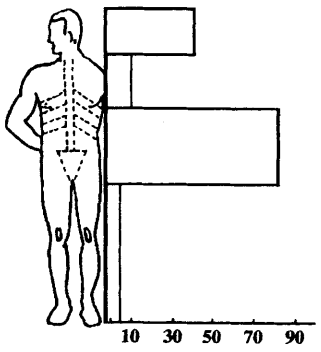

Fig. 33 Probable rates of survival after irradiation with a minimal absolute lethal dose as a function of body-shielding locations. From Refs. 120 and 121.

Radiation risks can be minimized in several ways. From an operational perspective, the length of an exposure in a radiation field can be managed, i.e., locations with lower dose rates are preferable over those with higher dose rates. Radiation risks can be mitigated during the design phase by adding additional shielding to attenuate radiation penetration from the exterior. Construction materials also can be selected in terms of their ability to minimize the production of secondary radiation, which in general means using materials with a lower mean nuclear charge. Specially designed body shielding (e.g., Fig. 33) can be used to protect specific organs, or a torso shield could be used to reduce whole-body exposures.

Other possible means of mitigating space radiation risks in the future involve radiation protectants, preirradiation conditioning, or postirradiation therapy, any or all of which may enhance tissue repair. If some people can be shown to be less prone to radiation damage than others or can repair damage more effectively, crews could be selected with these characteristics in mind.

Present research in chemical protection against radiation injuries includes developing new compounds of aminothiols, identifying immunomodulators, and using antioxidants. One well-known aminothiol compound, WR-2721, is effective against low-LET radiation but not high-LET neutrons. Some lipopolysaccharide endotoxins are potent immunostimulants, and can enhance a variety of immunopoietic and hemopoietic responses. Endogenous free-radical scavengers such as vitamins E, C, and A and glutathione are antioxidants. The effectiveness of these compounds against ionizing radiation depends on the concentrations used, the LET of the radiation, and the biological end point. In general, DNA damage by high-LET radiation is induced through direct action and is difficult to predict or protect against. Moreover, the consequences of using high concentrations of these compounds include nausea, vomiting, diarrhea, fever, hypotension, and hypocalcemia; these consequences must be circumvented before such compounds can be considered useful as radioprotectants. Some combinations of radioprotective agents have been found to reduce toxicity and produce synergistic protective effects in cosmonauts; further studies on the combined effects of several radioprotectants may prove fruitful. Several studies of radioprotectants as countermeasures to radiation exposure have been reported in the Russian literature.[121–124]

Although high concentrations of radioprotectants are necessary to inhibit lethal effects during irradiation, continuous treatment with relatively low concentrations of dimethyl sulfoxide (DMSO), e.g., 15.6%, has been found to reduce the effectiveness of x-rays by a factor of 3 for both cell inactivation and transformation. Cells treated continuously with 1% DMSO for 4 weeks after irradiation had the same transformation frequency as that of control cultures.[125] This type of postirradiation treatment also was effective for cells exposed to high-LET heavy ions. Similar results have been found with vitamins A and C. Compounds such as these may be useful against the carcinogenic effects of nonlethal doses of space radiation. Significant radioprotection probably can be achieved through a combination of nutrition, vitamin supplementation, and immunomodulation.

F. Uncertainties in Risk Assessments

The dose-equivalent to which an individual is exposed depends on three physical factors: the total flux of all types of radiation at a dose point in the human body; the LET distribution; and the quality factor for those radiation types. Thus, uncertainties arise from three sources as well: those related to the free-space radiation environment; those related to interactions of primary space radiation with space system material; and those related to the biological effects produced in humans.

Uncertainty in the free-space environment can arise from temporal variations if the specific duration of the exposure is unknown. For example, GCR fluxes in the 0.1 to 1 GeV/nucleon range can vary by an order of magnitude from solar maximum to solar minimum. The root-mean-square (rms) uncertainty in the GCR flux established by the model of Badhwar and O'Neill[37] is about 10%. Uncertainties introduced by transport calculations and secondary radiation production, although difficult to determine, are now being evaluated. The largest uncertainty, that of biological effects, is introduced by means of the quality factor, which is a defined quantity. If the quality factor is still a useful concept for heavy-ion effects, the uncertainty could be as much as 100%. Quantitative estimates of uncertainty are impossible because certain critically important measurements have yet to be made. We maintain that the first priority in reducing uncertainty in the risk estimate should be given to biology.

G. Ascertaining Acceptable Risks: Setting Dose Limits

The goal of one philosophy used to set exposure limits for ionizing radiation[126] is to limit the probability of radiation disease in exposed persons and their progeny to levels that justify the benefits of the activities that involve the exposure. Both stochastic and nonstochastic effects are considered in this approach. The objective is to prevent the occurrence of

nonstochastic effects by adhering to dose-equivalent limits that are less than the apparent threshold of the effect, and to limit the risk of stochastic effects to levels of comparable nonra-diation risks with comparable benefits to society.

Protection from space radiation assumes that risk is linearly proportional to the dose. Any activity involving radiation exposure will require justification, and exposures will be managed to levels that are as low as can be reasonably achieved. In other words, the effective dose-equivalent limit is the *upper* limit of acceptability rather than being a design criterion. The overall goal of the protection effort is to provide a level of protection for people who work with radiation that is comparable to that for workers in other "safe" industries. However, few industries introduce a risk of delayed stochastic effects such as cancer induction. Attempts have been made to relate radiation exposure risks to those of carcinogenic chemicals; however, the available data are too few for meaningful comparison. Consequently, the NCRP tends to relate radiation risks for terrestrial workers to that of accidental deaths in "safe" occupations, i.e., $< 10^{-4}$ /y. Less safe occupations are those with risks of accidental death greater than 10^{-4}/y, and substantially more hazardous occupations are defined as those that carry a risk of accidental death of more than 10^{-3}/y.

The National Council on Radiation Protection and Measurement[10] provides four considerations for limiting the late effects of radiation exposure: the risk of fatal cancer; the risk of serious genetic defects; the risk of cataracts; and fertility-related effects on gonads. Because nonradiation risks can never be eliminated entirely from space travel, radiation is considered an occupational risk. Nevertheless, astronauts and cosmonauts should not be subjected to an excess risk of late effects such as cancer when they have completed their flight careers.

Exposure limits are obtained for space crews by dividing the acceptable level of risk by the risk per Sv. For low-Earth-orbit flights, the NCRP adopted the middle group of "less-safe" occupations as an acceptable level of risk. Such occupations have lifetime risks of accidental death of about 3%. For this case, the dose limit for the risk of fatal cancer (0.04/Sv)[81] would be:

$$[\text{acceptable risk/risk} \cdot \text{Sv}^{-1}] = [0.03/0.04 \cdot \text{Sv}^{-1}] = 0.75 \text{ Sv}$$

Clearly, exposure limits depend on both a measured risk per dose-equivalent and administrative judgment that establishes an acceptable level of risk. The NCRP has yet to recommend an acceptable risk for exploration-class missions.

VII. Further Research Needed

Several areas clearly require considerably more research before meaningful risk assessments of space radiation can be made. Regarding trapped-belt models, a new dynamic model of the proton belts is needed that could incorporate spatial- and temporal-variation parameters, spectral changes, and descriptions and applications related to pitch angle. Several means of accounting for changes in the trapped-belt radiation environment have been proposed, the most accurate of which would be to update particle fluxes every 5 to 10 years with satellite measurements made in an equatorial or high-inclination orbit. Information on the pitch-angle distribution of the particles will be crucial; these data must be incorporated into the modified models to allow estimates of the directional doses obtained inside spacecraft with widely varying mass shielding solid-angle distributions. Proton particle energies studied should include the energy range 20–500 MeV.

Transport codes also are in need of additional development, particularly with regard to nuclear fragmentation cross-sections. Theoretical developments should be based on empirical data from ground-based studies involving particle accelerators. Additional research in radiation monitoring also is needed; decisions must be made as to the operational requirements for monitoring instruments and the programs necessary to develop the hardware.

The area of greatest uncertainty for developing risk assessments remains that of radiobiology and the human responses to high-energy protons and heavy ions. Data on cancer induction in humans by heavy ions are virtually nonexistent, and research is needed to determine the validity of extrapolating such data from animal subjects to humans. Radiobiological research also should be extended to examine other debilitating effects (e.g., brainstem damage) so that all of the risks associated with exposure to space radiation can be understood. Finally, results from these research efforts must be converted to operational procedures that can be used to minimize exposures when possible, and to counter the deleterious effects of space radiation when such exposures are unavoidable.

References

[1]Gazenko, O. G., Grigoriev, A. I., and Ilyin, Ye. A., "Medico-Biological Ensurance of Martian Manned Spaceflight," *Zemlya i Vselennaya,* No. 5, 1987, p. 15.

[2]Kovalov, Ye. Ye., Vikhrov, A. I., Petrov, V. M., et al., "Problems of Radiation Safety in Martian Manned Spaceflight," *Space Biology and Aerospace Medicine: 9th All-Union Conference,* Kaluga, June 19–21, 1990, Nauka, Moscow, 1990.

[3]Dudkin, V. E., Kovalov, Ye. Ye., Kolomensky, A. V., and Sakovich, V. A., "Radiation Shielding Estimates for Manned Mars Spaceflight" (IAF paper 90-544), *41st Congress of the International Astronautical Federation,* Dresden, Federal Republic of Germany, Oct. 6–12, 1990.

[4]Pisarenko, N. F., "Radiation Situation Determining the Possibility of a Manned Flight to Mars and Back," *Advances in Space Research,* Volume 12, No. 2, 1992, pp. 435–439.

[5]Badhwar, G. D., Hardy, A. C., McKay, D. S., Yang, T. C., Waligora, J. M., Abbott, B., and Richmond, R. G., "Radiation Assessment: Status and Issues for the First Lunar Outpost Mission," JSC Trade Study FLO-92, 1993.

[6]Robbins, D. E., "Radiation Health in Space," SAE Technical Series Paper No. 941615, *24th International Conference on Environmental Systems*, Friedrichshafen, Germany, June 20–23, 1994, Society of Automotive Engineers, Warrendale, PA, 1994.

[7]National Academy of Sciences/National Research Council (NAS/NRC), Radiobiological Advisory Panel, Committee on Space Medicine, *Radiation Protection Guides and Constraints for Space Mission and Vehicle Design Involving Nuclear Systems,* edited by W. H. Langham and D. Grahn, National Academy Press, Washington, DC, 1970.

[8]Petrov, V. M., Kolomensky, A. V., and Zil, M. V., "Radiation Dangers of Solar Flares in Earth Orbital Space 2: Evaluation of Dose and Risks of Exceeding," *Kosmicheskiye Isslendovanya,* Vol. 17, No. 1, 1979, pp. 122–126.

[9]GOST 25645.215-85, *Radiation Safety of Spacecraft Crews in Spaceflight: Safety Standards for Long Duration Flights up to Three Years,* Moscow, 1986, p. 14.

[10]National Council on Radiation Protection and Measurement (NCRP), *Guidance on Radiation Received in Space Activities,* NCRP Report No. 98, National Council on Radiation Protection and Measurements, Bethesda, MD, 1989.

[11]Antipov, V. V., Bayevsky, R. M., Gazenko, O. G., et al., "Some Recapitulations of Biomedical Investigations on the Second and Third Space Satellites," *Problemy Kosmicheskoi Biologii,* Vol. 1, 1962, p. 267.

[12]Warren, C. S., and Gill, W. L., "Radiation Dosimetry Aboard the Spacecraft of the Eighth Mercury-Atlas Mission (MA-8)," NASA Technical Note D-1862, NASA Manned Spacecraft Center, Houston, TX, 1964.

[13]Warren, C. S., and Baker, B. R., "Radiation Measurements on the Ninth Mercury-Atlas Mission (MA-9)," NASA Technical Note D-2608, NASA Manned Spacecraft Center, Houston, TX, 1964.

[14]Van Allen, J. A., "The First Public Lecture on the Discovery of Geomagnetically Trapped Radiation," Report 60-13, State University of Iowa Press, Ames, Iowa, 1960.

[15]McIlwain, C. E., "Coordinates for Mapping the Distribution of Magnetically Trapped Particles," *Journal of Geophysical Research,* Vol. 66, 1961, p. 3681.

[16]Noll, R. B., and McElroy, M. B., "The Earth's Trapped Radiation Belts: NASA Space Vehicle Design Criteria (Environment)," NASA SP-8116, NASA Goddard Space Flight Center, Greenbelt, MD, 1975.

[17]Reagan, J. B., Nightingale, R. W., Gaines, E. E., Imhof, W. L., and Stassinopoulos, E. G., "Outer Zone Energetic Electron Spectral Measurements," *18th Aerospace Sciences Meeting,* Pasadena, CA, January 14–16, 1980, 8 pp.

[18]Heckman, H. H., and Nakano, G. H., "East-West Asymmetry in the Flux of Mirroring Geomagnetically Trapped Protons," *Journal of Geophysical Research,* Vol. 68, 1963, p. 2117.

[19]Heckman, H. H., and Nakano, G. H., "Low-Altitude Trapped Protons during Solar Minimum Periods," *Journal of Geophysical Research,* Vol. 74, No. 14, 1969, pp. 3575–3590.

[20]Chapman, S., and Bartels, J., *Geomagnetism,* Oxford University Press, London, 1940.

[21]Lenchek, A. M., and Singer, S. F., "The Albedo Theory of Geomagnetically Trapped Protons: Investigating Intensity, Energy Spectrum, and Angular Distribution of Fast Neutrons," *Planetary and Space Science,* Vol. 11, 1963, pp. 1151–1208.

[22]Harmon, B. A., Fishman, G. J., Parnell, T. A., Benton, E. V., and Frank, A. L., "LDEF Radiation Measurements: Preliminary Results," *Nuclear Tracks and Radiation Measurements,* Vol. 20, No. 1, 1992, pp. 131–136.

[23]McIlwain, C. E., "The Radiation Belts: Natural and Artificial," *Science,* Vol. 142, 1963, pp. 355–361.

[24]Petrov, V. M., Panova, N. A., Shurshakov, V. A., Makhmutov, V. S., Dachev, Ts. P., and Semkova, J. V., "Experimental Investigations of Quasistatic Radiation Belts Formed After Solar Proton Events in September 1989 and March 1991 based on the 'Lyulin' Device Measurements aboard the Mir Space Station," *30th Topical Meeting of the Committee on Space Research (COSPAR),* Hamburg, Germany, July 1994, Report of Panel F2.7, Abstracts, Vol. II, p. 309.

[25]Lobakov, A. P., Lyagushin, V. I., Panasyuk, M. I., Shavrin, P. I., Makhmutov, V. S., Petrov, V. M., Shurshakov, V. A., Dachev, Ts. P., and Semkova, J. V., "Increase of Solar Cosmic Rays on the Mir Space Station in Orbit During Sept.-Oct. 1989," *Nuclear Tracks and Radiation Measurements,* Vol. 20, No. 1, 1992, pp. 59–64.

[26]Konradi, A., Badhwar, G. D., and Braby, L. A., "Recent Shuttle Observations of the South Atlantic Anomaly and Radiation Belt Models," *Advances in Space Research,* Vol. 14, No. 10, 1994, pp. 911–921.

[27]Robbins, D. E., and Badhwar, G. D., "Trapped Belt Variations and Their Effects on Human Space Flights," *44th Congress of the International Astronautical Federation,* Graz, Austria, Oct. 16–22, 1993.

[28]Sawyer, D. M., and Vette, J. I., "AP-8 Trapped-Proton Environment for Solar Maximum and Solar Minimum," NSSDC/WDC-A-R&S 76-6, National Space Science Center, Goddard Space Flight Center, Greenbelt, MD, 1976.

[29]Badhwar, G. D., and Konradi, A., "Conversion of Omnidirectional Proton Fluxes into a Pitch-Angle Distribution," *Journal of Spacecraft and Rockets,* Vol. 27, 1990, pp. 350–352.

[30]Teague, M. J., and Vette, J. I., "A Model of the Trapped-Electron Population for Solar Minimum," NSSDC 74-03, NASA National Space Science Data Center, Goddard Space Flight Center, Greenbelt, MD, 1974.

[31]Watts, J. W., Parnell, T. A., and Heckman, H. H., "Approximate Angular Distribution and Spectra for Geomagnetically Trapped Protons in Low-Earth Orbit," *High-Energy Radiation Background in Space,* edited by A. C. Rester, Jr. and J. I. Trombka, American Institute of Physics, New York, 1987, pp. 75–85.

[32]Golightly, M. J., Hardy, A. C., and Hardy, K. A., "Results of Time-Resolved Radiation Exposure Measurements Made during U.S. Shuttle Missions with a Tissue-Equivalent Proportional Counter," *28th World Congress on Space Research, COSPAR Plenary Conference,* Washington, DC, Aug. 28–Sept. 5, 1992.

[33]Hardy, A. C., Atwell, W., Richmond, R. G., and Cash, B. L., "Passive Radiation Dose Measurements Aboard the Space Shuttle," JSC-24076, NASA, Houston, TX, 1992.

[34]Richmond, R. G., Cash, B. L., Jones, K. L., and Mizner, A. A., "Operational Dosimetry for the Space Shuttle: A Short Summary of Techniques and Results," *Proceedings of the American Nuclear Society Topical Conference on Theory and Practice in Radiation Protection and Shielding,* ISBN: 0-89488-132-0, 1987.

[35]Mewaldt, R. A., "Elemental Composition and Energy Spectra of Galactic Cosmic Rays," *Interplanetary Particle Environment,* JPL Publication 88-28, edited by J. Feynman and S. Gabriel, NASA Jet Propulsion Laboratory, Pasadena, CA, 1988.

[36]Simpson, J. A., "Elemental and Isotopic Composition of the Galactic Cosmic Rays," *Annual Reviews of Nuclear and Particle Science,* Vol. 33, 1983, p. 706.

[37]Badhwar, G. D., and O'Neill, P. M., "An Improved Model of Galactic Cosmic Radiation for Space Exploration Missions," *Proceedings of the 22nd International Cosmic Ray Conference*, Dublin, Ireland, 1991.

[38]Badhwar, G. D., and O'Neill, P. M., "Long-Term Modulation of Galactic Cosmic Radiation and Its Model for Space Exploration," *Advances in Space Research,* Vol. 14, No. 10, 1994a, pp. 749–757.

[39]Badhwar, G. D., Cucinotta, F. A., and O'Neill, P. M., "An Analysis of Interplanetary Space Radiation Exposure for Various Solar Cycles," *Radiation Research,* Vol. 138, No. 2, 1994b, pp. 201–208.

[40]Adams, J. H. Jr., Badhwar, G. D., Mewaldt, R. A., Mitra, B., O'Neill, P. M., Ormes, J. F., Stemwedel, P., and Streitmatter, R. E., "The Absolute Spectra of Galactic Cosmic Rays at Solar Minimum and Their Implications for Manned Spaceflight," *Proceedings of the 22nd International Cosmic Ray Conference,* Dublin, Ireland, 1991.

[41]Mewaldt, R. A., Cummings, A. C., Adams, J. H. Jr., Evenson, P., Fillius, W., Jokipii, J. R., McKibben, R. B., and Robinson, P. A. Jr., "Toward a Descriptive Model of Galactic Cosmic Rays in the Heliosphere," *Interplanetary Particle Environment,* JPL Publication 88-28, edited by J. Feynman and S. Gabriel, NASA Jet Propulsion Laboratory, Pasadena, CA, 1988.

[42]Webber, W. R., *Workshop on the Space Radiation Environment,* NCRP Scientific Committee 75, National Council on Radiation Protection and Measurements, Bethesda, MD, 1991.

[43]Shea, M. A., "Intensity/Time Profiles of Solar Particle Events at One Astronomical Unit," *Interplanetary Particle Environment*, JPL Publication 88-28, edited by J. Feynman and S. Gabriel, NASA Jet Propulsion Laboratory, Pasadena, CA, 1988, pp. 75–84.

[44]Smart, D. F., "Predicting the Arrival Times of Solar Particles," *Interplanetary Particle Environment,* JPL Publication 88-28, edited by J. Feynman and S. Gabriel, NASA Jet Propulsion Laboratory, Pasadena, CA, 1988, pp. 101–110.

[45]Vahia, M. N., and Biswas, S., "Solar Energetic Particle Studies," *Composition and Origin of Cosmic Rays,* edited by M. M. Shapiro, Proceedings of the NATO Advanced Study Institute, Erice, Italy, June 20–30, 1983, Reidel Publishing, Dordrecht, The Netherlands, 1983, pp. 155–160.

[46]Feynman, J., Armstrong, T. P., Dao-Gibner, L., and Silverman, S., "New Interplanetary Proton Fluence Model," *Journal of Spacecraft and Rockets,* Vol. 27, 1990, pp. 403–410.

[47]Kolomenskiy, A. V., Petrov, V. M., Zil, M. V., and Yeremkina, T. M., "Radiation Danger from Solar Flares in Near-Earth Space. 1. Model-Based Description of Radiation Conditions," *Kosmicheskiye Issledovaniya,* Vol. 16, No. 5, 1978, pp. 698–704.

[48]Kudela, K., Zil, M. V., Kolomenskiy, A. V., Petrov, V. M., and Poradska, I., "The Use of Vertical Cut-Off Rigidities in Computations of Cosmic Ray Spectra on Earth Orbits," *Acta Physica Slovaca,* Vol. 36, 1986, pp. 319–324.

[49]Zil, M. V., Kolomenskiy, A. V., and Petrov, V. M., "Attenuation of the Dose of Solar Cosmic Radiation by the Earth's Magnetic Field," *Kosmicheskiye Issledovaniya,* Vol. 24, No. 7, 1986, pp. 944–947.

[50]Wilson, J. W., *Analysis of the Theory of High-Energy Ion Transport,* Report TN D-8381, NASA Langley Research Center, Langley, VA, 1977.

[51]Richmond, R. G., "The Space Radiation Environment and Its Measurement - From the Mercury Spacecraft to the Mars Mission," SAE Technical Series Paper No. 941614, *24th International Conference on Environmental Systems*, Friedrichshafen, Germany, June 20–23, 1994, Society of Automotive Engineers, Warrendale, PA, 1994.

[52]Richmond, R. G., and Hardy, A. C., "The Use of Passive Radiation Dosimeters in Monitoring the Space Radiation Environment," SAE Technical Series Paper No. 941613, *24th International Conference on Environmental Systems*, Friedrichshafen, Germany, June 20–23, 1994, Society of Automotive Engineers, Warrendale, PA, 1994.

[53]Jahnert, B., "The Response of TLE-700 Thermoluminescent Dosimeters to Protons and Alpha Particles," *Health Physics,* Vol. 23, No. 1, 1972, pp. 112–114.

[54]Henson, A. M., and Thomas, R. H., "Measurement of the Efficiency of Seven LiF Thermoluminescent Dosimeters of Heavy Ions," *Health Physics,* Vol. 34, 1978, pp. 389–390.

[55]Richmond, R. G., and Cash, B. L., "The Use of TLD at Very Low Doses," *Proceedings of the American Nuclear Society Topical Conference on Theory and Practice in Radiation Protection and Shielding*, ISBN: 0-89488-132-0, 1987.

[56]Benton, E. V., and Parnell, T. A., "Space Radiation and Dosimetry on U.S. and Soviet Manned Missions," *Terrestrial Space Radiation and Its Biological Effects,* edited by T. McCormack, C. E. Swenberg, and H. Bucker, NATO Advanced Studies Institute/Plenum Press, New York, 1988, p. 729.

[57]Vana, N., Schoner, W., Fugger, M., and Akatov, Y., "DOSIMir: A New Experimental Approach in Dose Equivalent Determination on Space Station Mir" (IAF/IAA-93-G.2.138), *44th Congress of the International Astronautical Federation,* Graz, Austria, Oct. 16–22, 1993.

[58]Vana, N., Schoner, W., Fugger, M., and Brandl, H., "Radiation Measurements on board High-Altitude Aircraft," *41st International Congress on Aviation and Space Medicine,* Hamburg, Germany, Sept. 12–16, 1993.

[59]Price, P. B., and Walker, R. M., "Observations of Charged Particle Tracks in Solids," *Journal of Applied Physics,* Vol. 33, 1962, pp. 3400–3408.

[60]Fleischer, R. L., Price, P. B., and Walker, R. M., *Nuclear Tracks in Solids: Principles and Applications,* University of California, Berkeley, CA, 1975.

[61]Fleischer, R. L., Price, P. B., and Walker, R. M., "Track Registration in Various Solid-State Nuclear Detectors" (abstract), *Physics Reviews A,* Vol. 133, 1964, p. 1443.

[62]Fleischer, R. L., Price, P. B., and Walker, R. M., "The Ion Explosion Spike Mechanism for Formation of Charged Particle Tracks in Solids," *Journal of Applied Physics,* Vol. 36, 1965, pp. 36–45.

[63]Katz, R., and Kobeitch, E. J., "Formation of Etchable Tracks in Dielectrics," *Physics Reviews,* Vol. 170, 1968, pp. 401–405.

[64]Benton, E. V., "On Latent Track Formation in Organic Nuclear Charged Particle Track Detectors," *Radiation Effects,* Vol. 2, 1970, pp. 273–280.

[65]International Commission on Radiological Protection and International Commission on Radiation Units and Measurements (ICRP-ICRU), "Report of the RBE Committee to the International Commissions on Radiological Protection and on Radiological Units and Measurements," *Health Physics,* Vol. 9, 1963, pp. 357–386.

[66]Benton, E. V., "A Study of Charged Particle Tracks in Cellulose Nitrate," Report USNRDL TR-68-14, U.S. Naval Radiological Defense Laboratory, San Francisco, CA, 1968.

[67]Rossi, H. H., "A Proposal for Revision of the Quality Factor," *Radiation and Environmental Biophyics,* Vol. 14, 1977, p. 275.

[68]Kellerer, A. M., and Rossi, H. H., "The Theory of Dual Radiation Action," *Current Topics in Radiation Research Quarterly,* Vol. 8, No. 2, 1985, pp. 85–158.

[69]Kellerer, A. M., "Fundamentals of Microdosimetry," *The Dosimetry of Ionizing Radiation,* edited by K. R. Kase, B. E. Bjarngard, and F. H. Attix, Vol. II, Academic Press, New York, 1989, pp. 78–108.

[70]Braby, L. A., "A Portable Dose-Equivalent Meter Based on Microdosimetry Techniques," *Nuclear Instruments and Methods in Physics Research,* Vol. B10-11, 1985, pp. 910–914.

[71]Nguyen, V. D., Bouisset, P., Parmentier, N., Akatov, I. A., and Petrov, V. M., "Real-Time Quality Factor and Dose-Equivalent Meter 'CIRCE' on Board the Soviet Space Station Mir," *Acta Astronautica,* Vol. 23, 1991, pp. 217–226.

[72]Badhwar, G. D., Konradi, A., Braby, L. A., Atwell, W., and Cucinotta, F. A., "Measurements of Trapped Protons and Cosmic Rays from Recent Shuttle Flights," *Radiation Protection Dosimetry,* Vol. 52, 1994, p. 439.

[73]Badhwar, G. D., Cucinotta, F. A., Braby, L. A., and Konradi, A., "Measurements on the Shuttle of the LET Spectra of Galactic Cosmic Radiation with the Radiation Transport Model," *Radiation Research,* Vol. 139, No. 3, 1994, pp. 344–351.

[74]Alpen, E. L., *Radiation Biophysics,* Prentice Hall, Englewood Cliffs, NJ, 1990.

[75]Fritz-Niggli, H., "The Role of Repair Processes in Cellular and Genetic Response to Radiation," *Terrestrial Space Radiation and Its Biological Effects,* edited by P. D. McCormack, C. E. Swenberg, and H. Bucker, NATO Advanced Study Institute/Plenum Press, New York, 1987.

[76]Rossi, H. H., "Specification of Radiation Quality," *Radiation Research,* Vol. 10, 1959, p. 522.

[77]International Commission on Radiological Protection (ICRP), "1990 Recommendations of the International Commission on Radiological Protection," ICRP Publication 60, also *Annals of the ICRP,* Vol. 21, No. 2, Pergamon Press, Oxford, 1991.

[78]International Commission on Radiological Protection (ICRP), "Recommendations of the International Commission on Radiological Protection," ICRP Publication 26, also *Annals of the ICRP,* Vol. 1, No. 3, Pergamon Press, New York, 1977.

[79]Robbins, D. E., and Yang, T. C., "Radiation and Radiobiology," *Space Physiology and Medicine,* 3rd ed., edited by A. E. Nicogossian, C. L. Huntoon, and S. L. Pool, Lea and Febiger, Philadelphia, 1994, pp. 167–193.

[80]Young, R. W., "Acute Radiation Syndrome," *Military Radiobiology,* edited by J. J. Conklin and R. I. Walker, Academic Press, New York, 1987, p. 166.

[81]United Nations Scientific Committee on the Effects of Atomic Radiation (UNSCEAR), *Sources, Effects and Risks of Ionizing Radiation,* Report to the General Assembly, with Annexes, United Nations, New York, 1988.

[82]National Academy of Sciences/National Research Council (NAS/NRC), *Health Effects of Exposure to Low Levels of Ionizing Radiation,* Report of the Committee on the Biological Effects of Ionizing Radiation, National Academy Press, Washington, DC, 1990.

[83]Pierce, D. A., and Vaeth, M., "The Shape of the Cancer Mortality Dose-Response Curve for A-Bomb Survivors," *Radiation Research,* Vol. 126, No. 1, 1991, pp. 36–42.

[84]Devine, R. T., and Chaput, R. L., "Low-Level Effects," *Military Radiobiology*, edited by J. J. Conklin and R. I. Walder, Academic Press, New York, 1987, pp 379–391.

[85]Keith, J. E., and Richmond, R. G., "Neutrons in Space: Measurements Aboard the Space Shuttle," *Proceedings of the American Nuclear Society Topical Conference on Theory and Practice in Radiation Protection and Shielding*, ISBN 0-89488-132-0, 1987.

[86]Keith, J. E., Badhwar, G. D., and Lindstrom, D. J., "Neutron Spectrum and Dose Equivalent in Shuttle during Solar Maximum," *Nuclear Tracks and Radiation Measurements,* Vol. 20, 1992, pp. 41–47.

[87]Keith, J. E., "Recent Neutron Measurements in Spacecraft," SAE Technical Series Paper No. 941617, *24th International Conference on Environmental Systems*, Friedrich-

shafen, Germany, June 20–23, 1994, Society of Automotive Engineers, Warrendale, PA, 1994.

[88]Petrov, V. M., Akatov, Y. A., Kozlova, S. B., Markelov, V. V., Nesterov, V. M., Redko, V. I., Smirenny, L. N., Khortsev, A. V., and Chernykh, I. V., "The Study of the Radiation Environment in Near-Earth Space: Dose Measurements by Kosmos Satellites," *17th COSPAR Plenary Meeting,* Sao Paulo, Brazil, June 17–July 1, 1975, *Life Sciences and Space Research,* Vol. 13, 1975, pp. 129–134.

[89]Badhwar, G. D., Braby, L. A., and Konradi, A., "Real-Time Measurements of Dose and Quality Factors Onboard the Space Shuttle," *Nuclear Tracks and Radiation Measurements,* Vol. 17, No. 4, 1991A, pp. 591–594.

[90]Badhwar, G. D., Braby, L. A., Cucinotta, F. A., and Atwell, W., "Dose Rate, Dose-Equivalent Rate, and Quality Factor in SLS-1," *Nuclear Tracks and Radiation Measurements,* Vol. 20, 1991, pp. 447–451.

[91]Badhwar, G. D., Konradi, A., Hardy, A. C., and Braby, L. A., "Active Dosimetric Measurements on Shuttle Flights," *Nuclear Tracks and Radiation Measurements,* Vol. 20, 1992, pp. 13–20.

[92]Adams, J. H. Jr., "Cosmic Ray Effects on Microelectronics," Memorandum Report 5901, Part IV, Naval Research Laboratory, Washington, DC, 1986.

[93]Simonsen, L. C., and Nealy, J. E., "Radiation Protection for Human Missions to the Moon and Mars," NASA TM-3079, NASA Langley Research Center, Langley, VA, 1991.

[94]Simonsen, L. C., Nealy, J. E., Sauer, H. H., and Townsend, L. W., "Solar Flare Protection for Manned Lunar Missions: Analysis of the October 1989 Proton Flare Event," SAE Technical Series Paper No. 911351, *21st International Conference on Environmental Systems*, San Francisco, CA, July 15–18, 1991, Warrendale, PA, 1991.

[95]Letaw, J. R., Silberberg, R., and Tsao, C. H., *Terrestrial Space Radiation and Its Biological Effects,* edited by P. D. McCormack, C. E. Swenberg, and H. Bucker, NATO Advanced Studies Institute/Plenum Press, New York, 1988.

[96]Curtis, S. B., and Letaw, J. R., "Galactic Cosmic Rays and Cell-Hit Frequencies Outside the Magnetosphere," *Advances in Space Research,* Vol. 9, No. 10, 1989, pp. 293–298.

[97]Townsend, L. W., Shinn, J. L., and Wilson, J. W., "Interplanetary Crew Exposure Estimates for the August 1972 and October 1989 Solar Particle Events," *Radiation Research,* Vol. 126, 1991, pp. 108–110.

[98]Benghin, V. V., Petrov, V. M., Taltson, M. V., Chernykh, I. V., and Shumshuron, V. I., "Dosimetric Control Onboard the Mir Space Station During the Solar Proton Events of Sept.–Oct. 1989," *Nuclear Tracks and Radiation Measurements,* Vol. 20, No. 1, 1992, pp. 21–23.

[99]National Council on Radiation Protection and Measurements (NCRP), "Influence of Dose and its Distribution in Time on Dose-Response Relationships for Low-LET Radiation," NCRP Report No. 64, Bethesda, MD, 1980.

[100]Grahn, D., *HZE Particle Effects in Manned Space Flight,* Radiobiological Advisory Panel Committee on Space Medicine, National Academy of Sciences, National Academy Press, Washington, DC, 1973.

[101]Fry, R. J. M., Powers-Risius, P., Alpen, E. L., and Ainsworth, E. J., "High-LET Radiation Carcinogenesis," *Radiation Research,* Suppl. No. 8, 1985, pp. S188–S195.

[102]Curtis, S. B., Townsend, L. W., Wilson, J. W., Powers-Risius, P., Alpen, E. L., and Fry, R. J. M., "Fluence-Related Risk Coefficients Using the Harderian Gland Data as an Example," *Advances in Space Research,* Vol. 12, No. 2–3, 1992, pp. 407–416.

[103]Vogel, H. H. Jr., and Dickson, H. W., "Mammary Neoplasia in Sprague-Dawley Rats Following Acute and Protracted Irradiation," *Neutron Carcinogenesis,* edited by J. J. Broerse and G. B. Gerber, Commission of the European Communities, Luxembourg, 1982.

[104]Burns, F. J., and Albert, R. E., "The Dose Response for Rat Skin Tumor Induction Estimated from Multiple Doses" (abstract), *Radiation Research,* Vol. 83, No. 2, 1981, p. 435.

[105]Burns, F. J., Hosselet, S., and Garte, S., "Extrapolation of Rat Skin Tumor Incidence: Dose Fractionation and Linear Energy Transfer," *Proceedings of the 14th L. H. Gray Conference: Low Dose Radiation: Biological Bases of Risk Assessments,* Taylor and Francis, London, 1989.

[106]Yang, T. C., Craise, L. M., Mei, M., and Tobias, C. A., "Neoplastic Cell Transformation by Heavy Charged Particles," *Radiation Research,* Vol. 104, 1985, pp. S177–S187.

[107]Suzuki, M., Watanabe, M., Suzuki, K., Nakano, K., and Kaneko, I., "Neoplastic Cell Transformation by Heavy Ions," *Radiation Research,* Vol. 120, 1989, pp. 468–476.

[108]Hei, T. K., and Hall, E. J., "In Vitro Oncogenic Transformation at Low Doses and Relevance to Human Cancer Induction," *Cell Transformation Systems Relevant to Radiation-Induced Cancer in Man,* edited by K. H. Chadwick, C. Seymour, and B. Barnhart, Adam Hilger, NY, 1989, p. 349.

[109]Borek, C., Hall, E. J., and Rossi, H. H., "Malignant Transformation in Cultured Hamster Embryo Cells Produced by X-Rays, 460 keV Monoenergetic Neutrons, and Heavy Ions," *Cancer Research,* Vol. 38, 1978, pp. 2997–3005.

[110]Yang, T. C., Craise, L. M., Mei, M., and Tobias, C. A., "Dose Protraction Studies with Low- and High-LET Radiation on Neoplastic Cell Transformation In Vitro," *Advances in Space Research,* Vol. 6, 1986, pp. 137–147.

[111]Hill, C. K., Buonagura, F. M., Meyers, C. P., Han, A., and Elkind, M. M., "Fission-Spectrum Neutrons at Reduced Dose Rates Enhance Neoplastic Transformation," *Nature,* Vol. 298, 1982, pp. 67–69.

[112]Miller, R. C., Brenner, D. J., Geard, C. R., Komatsu, K., Marino, S. A., and Hall, E. J., "Oncogenic Transformation by Fractionated Doses of Neutrons," *Radiation Research,* Vol. 114, No. 3, 1988, pp. 589–598.

[113]Charles, M., Cox, R., Goodhead, D., and Wilson, A., "Meeting Report of CEIR Forum on the Effects of High-LET Radiation at Low Doses/Dose Rates," *International Journal of Radiation Biology,* Vol. 58, No. 5, 1990, p. 859.

[114]Crompton, N. E. A., Barth, B., and Keifer, J., "Inverse Dose Rate Effect for the Induction of 6-Thioguanine-Resis-

tant Mutants in Chinese Hamster V79-S Cells by Cobalt-60 Gamma Rays," *Radiation Research,* Vol. 124, 1991, pp. 300–308.

[115]Borek, C., "Radiation Oncogenesis in Cell Culture," *Advances in Cancer Research,* Vol. 37, 1982, pp. 159–232.

[116]Namba, M., Nishitani, K., Kimoto, T., and Sato, K., "Multistep Neoplastic Transformation of Normal Human Fibroblasts and Its Genetic Aspects," *Cell Transformation Systems Relevant to Radiation-Induced Cancer in Man,* edited by K. H. Chadwick, C. Seymour, and B. Barnhart, Adam Hilger, New York, 1984.

[117]Redpath, J. L., Sun, C., Colman, M., and Stanbridge, E. J., "Neoplastic Transformation of Human Hybrid Cells by Gamma Radiation: A Quantitative Assay," *Radiation Research,* Vol. 110, No. 3, 1987, pp. 468–472.

[118]Yang, T. C., Craise, L. M., and Tobias, C. A., "Molecular Lesions Important for Neoplastic Cell Transformation of Mouse (C3H10T1/2) and Human Epithelial Cells by Ionizing Radiation," *Cell Transformation Systems Relevant to Radiation Induced Cancer in Man,* edited by K. H. Chadwick, C. Seymour, and B. Barnhart, Adam Hilger, New York, 1989, pp. 301–308.

[119]Yang, T. C., Craise, L. M., Prioleau, J. C., Stampfer, M. R., and Rhim, J. S., "Chromosomal Changes in Cultured Human-Epithelial Cells Transformed by Low- and High-LET Radiation," *27th World Congress on Space Research, COSPAR Plenary Conference,* Hague, The Netherlands, June 25–July 6, 1990.

[120]Saksonov, P. P., Antipov, V. V., and Davydov, B. I., "Notes on Space Radiobiology," *Problemy Kosmicheskoi Biologii,* Vol. 9, Nauka, Moscow, 1968, 532 pages (in Russian).

[121]Antipov, V. V., and Ushakov, I. B., "Ionizing Radiation," *Aviation Medicine Manual,* Meditsina, Moscow, 1986, pp. 242–265.

[122]Antipov, V. V., Davydov, B. I., Ushakov, I. B., and Fedorov, V. P., *Effects of Spaceflight Factors on the Central Nervous System: Structural-Functional Aspects of Radio-Modification Influence,* Nauka, Moscow, 1989, 328 pp.

[123]Kirillov, V. F., Knizhnikov, V. A., and Korenkov, I. P., *Radiation Hygiene,* Meditsina, Moscow, 1988.

[124]Ilyin, L. A., Suvuruv, N. N., Chernov, G. A., et al., "Indralin: A New Radioprotector of Instant Action (Radioprotective Qualities, Phamacology, Mechanisms of Action)," *Radiobiol. syezd. Tez. doke. 2 syezda radiobioogov SNG,* Pt. 1, Pushtshino RAN, p. 410.

[125]Yang, T. C., and Tobias, C. A., "Neoplastic Cell Transformation by Energetic Heavy Ions and Its Modification with Chemical Agents," *Advances in Space Research,* Vol. 4, 1984, pp. 207–218.

[126]National Council on Radiation Protection and Measurements (NCRP), "Recommendations on Limits for Exposure to Ionizing Radiation," NCRP Report No. 91, Bethesda, MD, 1987.